LUND UNIVERSITY

Development and evaluation of an independent system for absorbed dose calculations in radiotherapy

Johnsson, Stefan

2003

Development and Evaluation of an Independent System for Absorbed Dose Calculations in Radiotherapy

Stefan Johnsson

Department of Radiation Physics
The Jubileum Institute
Lund University
2003

FACULTY OF MEDICINE
Lund University

Thesis for the degree of Doctor of Philosophy, Faculty of Medicine
Lund University
The Jubileum Institute, Department of Radiation Physics
Lund University Hospital
SE-221 85 Lund, SWEDEN

ISBN 91-628-5498-4
Printed in Sweden by KFS i Lund AB, Lund, 2003

ABSTRACT

The aim of this work was to develop, implement and evaluate an independent system with which to calculate the absorbed dose, delivered by high-energy X-ray beams, to the prescription point and the depth of dose maximum. The introduction of such a system in the clinical routine may help ensure high-quality treatment and avoidance of errors which may jeopardise the clinical outcome of the treatment (i.e. under- or overdose). A set of equations for calculating the absorbed dose to the prescription point was compiled in a software application ("HandCalc"), which is completely independent of the treatment planning system (TPS). For instance, HandCalc includes models to calculate the absorbed dose from photons scattered in the patient, the transmission of the primary kerma in the patient, the variation of the primary kerma in air with collimator setting (i.e. head scatter), and corrections for heterogeneities in the patient. A new expression for the transmission of the primary kerma in the patient was derived in which the coefficients are strictly defined (and given a physical interpretation) by the first two moments of the spectral distribution of the incident beam. Further investigations also revealed that these moments can be used to determine water-to-air stopping power ratios more accurately than other beam quality indices. In practice, the moments are derived from "in-air equivalent", narrow-beam measurements using a mini-phantom. The degree of in-air equivalence was investigated with Monte Carlo simulations, which showed that the optimum measurement depth in a mini-phantom is somewhat below the depth of dose maximum. Based upon comparisons with measurements and the TPS, a clinical action level of ±4% was chosen for HandCalc. Deviations greater than this are, with all probability, due to erroneous handling of the patient dataset during the preparation phase. An "entrance dose factor" was added in order to correct the dose calculations at the depth of dose maximum where electron equilibrium has not been established. The entrance dose factor was found to vary with beam quality and collimator setting, while no variation was detected with the presence of an acrylic tray (for block support) or with the source-surface distance (SSD). HandCalc was implemented in a hand-held PC which makes dose calculations inside the treatment room at the time of administration of the first fraction possible. An important feature of HandCalc is the built-in report function, which logs results from the calculation for later evaluation. In a study including 700 patients, deviations greater than the action level were found to be due either to limitations in HandCalc or to a systematic deviation between the planned and measured SSD. HandCalc has proven to be a fast and accurate tool for independent dose calculations inside the treatment room and it requires only a limited amount of extra time for the user to perform the calculations. Thus, it can easily be incorporated as part of the daily clinical quality control programme in order to prevent errors which may jeopardise the clinical outcome of the treatment.

Keywords: radiation therapy, dose calculation, monitor unit calculation, error prevention, quality control, beam quality, stopping power ratio, entrance dose, primary kerma, transmission measurement, in-air equivalence, mini-phantom, PDA

LIST OF ORIGINAL PAPERS

This thesis is based on studies reported in the following papers, referred to in the text by their Roman numerals.

I. **Johnsson SA**, Ceberg CP, Knöös T and Nilsson P: Transmission Measurements in Air using the ESTRO Mini-phantom. *Phys. Med. Biol.* **44 (10)**: 2445-2450, 1999.

II. **Johnsson SA**, Ceberg CP, Knöös T and Nilsson P: On Beam Quality and Stopping Power Ratios for High-Energy X-rays. *Phys. Med. Biol.* **45 (10):** 2733-2745, 2000.

III. Knöös T, **Johnsson SA**, Ceberg CP, Tomaszewicz A and Nilsson P. Independent Checking of the Delivered Dose for High-Energy X-rays Using a Hand-Held PC. *Radiother Oncol.* **58 (2):** 201-208, 2001.

IV. **Johnsson SA,** Ceberg CP and Nilsson P. A Simplistic Formalism for Calculating Entrance Dose in High-Energy X-ray Beams. *Phys. Med. Biol.* **47 (22):** 3985-3997, 2002.

V. **Johnsson SA** and Ceberg CP. Evaluation of an Independent System for Dose Calculations using a Hand-Held PC. Manuscript to be submitted.

Table of contents

1. INTRODUCTION

1.1 Background

The requirements on the delivery of the prescribed dose to the target in radical radiation therapy using high-energy X-ray beams are extremely high, both in terms of spatial accuracy and in dosimetry. It has been reported that the combined standard uncertainty in dose delivery should be in the interval 3-5% in order not to jeopardise the clinical outcome of the treatment (i.e. under- or overdose) [1-8]. Commercial vendors and users have successfully managed to implement radiation therapy systems which are able to achieve these demands with high accuracy and reproducibility. These systems include fixation devices, computerized tomography (CT) scanners, treatment planning systems (TPS), simulators, treatment machines, electronic portal imaging devices (EPID) and record and verify (R&V) systems. Computer networks are also becoming more common for ensuring data integrity when transferring information between systems. Extensive checks and analyses are usually performed at each clinic prior to the clinical use of each newly introduced system in the treatment chain. Normally, these checks are directed at a specific system, where the unit in question is regarded as an isolated part of the chain. Some inter-system tests regarding transfer of data between individual systems may also be performed to ensure the integrity of the dataset. For example, the transfer of data from the TPS to the R&V system and finally to the treatment unit may be accomplished. System-specific tests covering the whole process are, however, rare, and no methods are at present recommended.

Even if the systems described above are commissioned and subjected to quality assurance programmes to maintain their accuracy, errors may be introduced. Especially the human factor is an uncontrolled parameter that may introduce errors. During clinical routine, data regarding the patient's treatment (both geometric and dosimetric) are used at several stations, either for some kind of action at the TPS, simulator, and/or at the accelerator, or for review by, for example, the radiation oncologist at a workstation. At each station, data are available for editing and the addition of complementary information. The relevance and consistency of these intentional data changes might not always be clear to the specific user, which may result in undesirable consequences. In addition, unintentional changes may occur at any stage during the treatment chain, and there may also be errors in the data transfer process. At the treatment unit, the absorbed dose to be delivered to the patient is always given by the dataset present in the computer controlling

the treatment unit. The most important parameter is the number of monitor units (MUs), which have been calculated using either data tables (i.e. "manual plans") or within the TPS (i.e. "3D dose plans" or "TPS plans"). Thus, changes that have "slipped" into the patient dataset earlier in the preparation phase may lead to errors which are repeated with every fraction and thus influence the total dose delivered to the patient. It has been shown that errors were present in 15% of the datasets (studied), either at the compilation of the plan or at the execution of the first treatment [9]. Another study showed that erroneous data transfer affected 26% of the treatments and that a major deviation (i.e. >5%) occurred in 5% of the new treatments [10]. In a more recent pilot study by Verstraete and Huyskens, it was reported that at least one error was detected for more than 40% of the patients [11]. The vast majority (60%) of these errors were generated in the planning process. Most errors were detected before treatment, but errors in the actual treatment were detected for 10% of the patients. Studies where the main focus is on the origin of the detected errors can also be found in the literature [12, 13]. Thus, methods of detecting these errors and improving the quality of treatment are highly desirable.

Combined with an *in vivo* dosimetry system (which will not be considered in this thesis), an independent system which utilizes the final patient dataset to calculate the absorbed dose to the prescription point may help ensure that the patient (with a high probability) receives the correct dose prescribed by the radiation oncologist. Such a system can be used to find both systematic and random errors in dosimetry. Systematic errors in this context are errors present for a group of patients, e.g. errors in beam data for a specific treatment machine or geometric distortion during CT due to a specific immobilization device. Random errors are defined as those that affect the individual patient[1]. These errors are often due to human mistakes and include transcription errors, rounding-off errors, forgotten data or interchange of data in the handling of the patient dataset during the preparation phase.

An independent calculation system has been used by Williams *et al.* [14], who reported a deviation in absorbed dose of 2% or more in 2% of the checked plans, and a 5% deviation or more in 0.5% of the plans. Similar studies have been performed by Calandrino *et al.* [15, 16], where an independent manual check was used to measure the human error rate in the calculation of monitor units. A serious error (i.e. dose deviations greater than 5%) was found in 1.3% and 0.74% of the checked plans in the two studies. In another study by Duggan *et al.* [17], errors greater than 5% were found in

[1] Note that the distinction between systematic and random errors differs compared to the distinction used in e.g. the IAEA protocol for absolute dosimetry [5].

0.3% of all the cases checked. Furthermore, Hill *et al.* found a number of significant errors in the TPS when an independent monitor unit calculation system was used [18]. Recommendations to use an independent dose calculation procedure can also be found in publications from AAPM [19, 20] and ESTRO [4, 21] and in national regulations[2].

Although the main purpose of an independent calculation system is to reveal human errors which can potentially lead to under-/over-dosages to the patient, it can also serve as an instrument to evaluate existing quality control routines, e.g. double manual checks of the treatment chart, MU calculations and the R&V system.

1.2 Requirements

By combining the dosimetry estimates of Andreo [22] with the delivery estimates of Brahme [2], Ahnesjö and Aspradakis [23] suggested that dose calculations need not be better than 2% (1 SD) with a correction action level of 4%. With present techniques and equipment, this would result in an overall uncertainty in the delivered dose to the patient of 4.6% (1 SD). With future developments in calibration[3] and in the delivery of absorbed dose, this overall uncertainty can be reduced to 3.1% (1 SD) if the accuracy in the dose calculation is kept constant. It must be emphasized, however, that these estimates only include uncertainties in dosimetry and not in geometry (e.g. target delineation).

An accuracy of 2% in an independent dose calculation system requires a very sophisticated calculation model if the system is to be versatile and function properly in both simple and complex beam geometries, e.g. with irregular field shapes, off-axis calculations, asymmetric fields, dynamic wedges, and in heterogeneous media. Ideally, the model should also be able to calculate the dose at the depth of dose maximum (d_{max}), i.e. the entrance dose, in order to allow comparison with *in vivo* measurements. These calculations are generally more difficult than the corresponding calculations at the prescription point due to, for example, contaminating electrons from the treatment head and the intervening air gap.

The simplest solution (and probably the most common) is to use existing tables of depth doses and output factors and to perform manual calculations assuming the patient to be a homogeneous water phantom. Besides being less accurate in more complex beam geometries (e.g. in a heterogeneous

[2] The Swedish Radiation Protection Authority's Regulations (SSI FS 2000:4) on Radiation Therapy (http://www.ssi.se/forfattning/PDF_Eng/2000-4e.PDF)

[3] The uncertainties in calibration can be reduced if the ionisation chamber is calibrated directly in water in terms of the absorbed dose to water [5, 24].

medium), this is also a rather slow method if calculations have to be carried out for a number of fields. It may also be argued that this type of calculation is not completely independent since the same physical data may have been used earlier in the preparation phase (at least for manual plans). A more elaborate solution (including corrections for heterogeneities and off-axis positions) has been proposed by, for example, Leszczynski and Dunscombe, and by Hill *et al.* [18, 25], where an MS Excel™ spreadsheet is used to speed up the calculations.

The most sophisticated solution, on the other hand, would be to use an independent TPS to calculate the dose just before the patient receives his/her first treatment. Although attractive in theory (due to its high accuracy), this solution is too expensive for most clinics, both economically and practically. In addition, since the optimum location for performing an independent calculation is inside the treatment room during the setup of the first treatment (using the actual patient dataset), the current calculation speed of most TPS computers makes this a time-consuming task. Thus, a cheaper and more efficient calculation system is needed.

One basic physical principle in photon dose calculations which has enjoyed considerable success involves the separation of the total absorbed dose into its primary and secondary components. This concept has been used, for example, in the ESTRO Booklets, Nos. 3 and 6 [4, 21], where a procedure for monitor unit calculations for radiation treatment with photon beams from linear accelerators and ^{60}Co units is presented. The formalism is based on measurements, and it is applicable to most practical situations encountered in radiotherapy applying rectangular, blocked and wedged beams, both under isocentric and fixed source-skin distance conditions. At the present time, however, the formalism does not include asymmetric fields, off-axis calculations, dynamic wedges and entrance dose calculations. Furthermore, an extensive set of measurements, both in a mini-phantom and in a large water phantom, must be performed before the system can be used clinically. Naturally, extra measurements are needed in order to determine the parameters for an independent system, but to reduce the amount of work, a model which requires a minimum number of extra measurements is desirable. Despite these shortcomings, the formalism proposed by ESTRO has the potential to become the unifying method with which to aid communication between departments. It has already found widespread acceptance, and future development of the formalism [26, 27] will certainly make it attractive as a basis for independent dose calculations. The accuracy of the ESTRO formalism is stated to be around 1-2% for the supported beam geometries.

Another interesting formalism in which the absorbed dose to the patient is separated into its primary and scattered components has been proposed by

Bjärngard and co-workers [28-31]. This semi-empirical formalism is accurate in standard beam geometries (around 1%), and only requires a minimum number of extra measurements [32]. It also has the potential for use in more complex beam geometries where, for example, pencil-beam calculations are required [33, 34]. Due to these attractive features, this formalism has been adopted as a basis for the calculation model in this work. The central part of this formalism is constituted by the dose-weighted average linear attenuation coefficient, which is used as a beam quality specifier in the determination of the scattered dose and the transmission of primary photons in the patient, the latter in combination with a beam-hardening coefficient. These coefficients are extracted from in-air equivalent, narrow-beam measurements using a mini-phantom. It has to be further investigated, however, if these measurements really are in-air equivalent since both attenuation of primary photons and build-up of scattered photons will take place in the mini-phantom. It is also desirable to find a more stringent representation of the transmission of primary photons where the coefficients are given a clear and unique physical interpretation. If this is possible, these coefficients may form a new and better method for characterising beam quality in high-energy photon beams. One drawback of the formalism is the requirement of transient electronic equilibrium for the derivation of scattered dose, which limits its accuracy at depths close to the surface, where the entrance dose is calculated. Thus, the current formalism must be improved in order for it to be a versatile and complete tool for independent dose calculations.

As mentioned above, the optimal location for performing an independent calculation is inside the treatment room while the patient is being set up for his/her first treatment. With this approach, late errors which have slipped into the system can be detected before the treatment starts. Although it is possible to implement any of the calculation methods mentioned above in a stationary PC, a more flexible solution would be to use a small hand-held computer, i.e. a personal digital assistant (PDA). A PDA can easily be used inside the treatment room and it is powerful enough to perform advanced calculations instantly while the patient is on the couch. The versatility and mobility of PDAs also make them interesting tools for other fields in radiotherapy. Together with the appropriate software, they can be used as a tool in external audits and in satellite clinics where flexibility and accuracy are crucial. In combination with equipment for wireless communication, a PDA can also be used as a mobile extension of the R&V system, where important information about the patient can be viewed at any time or place.

1.3 Objectives

The overall objective of the work described in this thesis was to develop, implement and evaluate an independent system with which to calculate the absorbed dose, delivered by high-energy X-ray beams, to the prescription point and the depth of dose maximum. The accuracy was required to be 1 and 2% (1 SD) compared with standard measurements and a TPS, respectively.

The specific objectives concerning the calculation model were to eliminate the limitations mentioned in the introduction. These objectives can be summarized as follows:

- To develop a new expression for the transmission of the primary kerma in water where the parameters are uniquely correlated to the spectral distribution of the incident beam.
- To show that these parameters form a new method of characterising beam quality which works satisfactorily over the entire range of energies and accelerators used in radiotherapy.
- To define and explain the concept of in-air equivalence in order to determine if transmission measurements using a mini-phantom are in-air equivalent.
- To develop a new formalism to correct for the effect of electron disequilibrium at the depth of dose maximum.

The implementation and evaluation of the system as a tool in the daily quality control process included the following specific objectives:

- To determine an action level for the calculation system. This was accomplished by comparing the dose calculation model with measurements and a commercial TPS.
- To implement the system in a hand-held PC in order to perform calculations inside the treatment room in a fast, simple and intuitive way while the patient is being prepared for his/her first treatment.
- To test the system in routine clinical work in order to reveal errors in the patient dataset, to investigate if the action level has been adequately chosen and to evaluate existing quality control routines in the department.
- To investigate other fields of application for a hand-held PC.

2. THE CALCULATION MODEL

The calculation model used in this work is based on the separation of the total absorbed dose (D) into its primary and secondary components (subscripts P and S, respectively):

$$D = D_P + D_S \tag{1a}$$

The primary dose in this context is the dose deposited by electrons generated by photons that have not interacted previously in the irradiated medium, while the "secondary" (or scattered) dose originates from electrons produced by photons that have already interacted at least once in the medium. By using the dose-to-kerma ratio [35, 36], β, the total dose can be written as:

$$D = \beta_P K_P + \beta_S K_S \tag{1b}$$

By choosing the kerma[4] rather than absorbed dose, effects associated with the propagation of the secondary electrons are dealt with separately through the ratio β. As the scattered dose is either very low or nearly equal to "scatter kerma" [36], it is generally justified to set β_S=1. We then assume that the field size is large enough to ensure lateral electronic equilibrium (i.e. ≥5x5 cm^2 for the energies used in this work) [37, 38], and that the recommendations given by ICRU for prescribing and reporting absorbed dose are followed, i.e. the prescription point should be positioned in a region without steep dose gradients, and preferably close to the centre of the planning target volume [6, 39, 40]. Thus, for all clinical cases, the prescription point is positioned in areas where transient electronic equilibrium is established, which is where β_P can be set equal to unity [36]. By defining the scatter-to-primary kerma ratio [28], $\sigma=K_S/K_P$, the total dose can be written as:

$$D = K_p(1+\sigma) \tag{1c}$$

The primary kerma can be further separated into two factors:

$$K_P = K_{P,0} \cdot T\,, \tag{2}$$

[4] Kerma refers to the total kerma and not only the collision part of the kerma.

where T is the transmission factor, which accounts for the attenuation of the primary kerma in the medium. The primary kerma "free in air", $K_{P,0}$, is the resulting primary kerma at the calculation point if the surrounding medium were removed. The primary kerma "free in air" relative to a reference field, $K_{P,0}^{rel}=K_{P,0} / K_{P,0,ref}$, is a measurable quantity, and depends on the collimator setting, c, defined at the isocentre (the head-scatter factor, $H(c)$), the distance, f, from the X-ray source (the inverse square law, $I(f)$), and the presence of a shadow tray for block support (the transmission factor of the shadow tray, $k'_{o,t}(c)$):

$$K_{P,0}^{rel}(c,f) = H(c) \cdot I(f) \cdot k'_{o,t}(c) \tag{3}$$

By relating the dose per monitor unit (D/M) to a reference situation (e.g. that used for calibrating the treatment unit in terms of absolute absorbed dose per monitor unit [5, 41]), the final expression for the absorbed dose in the medium can be written as:

$$D = M\left(\frac{D}{M}\right)_{ref} K_{P,0}^{rel} \frac{T}{T_{ref}} \frac{(1+\sigma)}{(1+\sigma_{ref})} \text{ [Gy]}, \tag{4}$$

where M is the number of monitor units for the actual field. Note that in the present form, Equations (3-4) only support calculations on the central axis. Absorbed dose calculations at positions off the central axis will be discussed later.

2.1 The transmission factor

The transmission factor, $T(z)$, describes the relative decrease in the primary kerma with depth, z, in the medium due to the attenuation of the primary photons, i.e. $T(z)=K_p(z)/K_p(0)$. Since the beam from a medical linear accelerator is not monoenergetic, beam-hardening effects will take place, i.e. photons with lower energies will be more attenuated than photons with higher energies (a valid assumption for the energies considered in this work). According to Bjärngard and Shackford [29], the transmission of primary dose is best described by a second-order exponential using a dose-averaged linear attenuation coefficient, μ, and a beam-hardening coefficient, η. Unfortunately, there are no precise definitions of these coefficients for polyenergetic spectra allowing a clear physical interpretation. Under certain conditions, however, μ and η can be identified with the first two moments

of the spectral distribution[5]. This concept has been adopted in spectral reconstruction methods using the inverse Laplace transform of transmission curves. For instance, Huang *et al.* [42] used the mean and the standard deviation of a Gaussian spectrum (distributed in μ) as parameters in their description of the transmission curve. While Huang *et al.* only considered Gaussian representations of the spectral distribution, a correlation between the moments of the spectral distribution and the transmission curve was derived for any (continuous) spectral distribution in **Paper II**:

$$T(z) = \exp\left(\sum_{i=1}^{\infty} a_i z^i \right) \tag{5a}$$

The coefficients a_i are given by:

$$a_i = \frac{(-1)^i \kappa_i}{i!} \tag{5b}$$

where κ_i is the cumulant of order i, given by the recursive formula:

$$\kappa_i = E\left[\mu^i\right] - \sum_{n=1}^{i-1} \binom{i-1}{n} \kappa_{i-n} E\left[\mu^n\right] \tag{5c}$$

Thus, the coefficients in the exponential are strictly defined (and given a physical interpretation) by the moments $E[\mu^i]$ of the spectral distribution of the incident beam. This spectral distribution is represented by $f(\mu)$, which is the relative primary kerma differentiated with respect to μ (see Equation (3) in **Paper II**). The derivation of Equation (5) was rather straightforward once $f(\mu)$ was formed and identified as a moment-generating function. An example of $f(\mu)$ for a 6 MV open beam is given in Figure 1.

[5] The nth moment of the function $f(x)$ is defined as: $E[x^n] = \int x^n f(x)\, dx$.

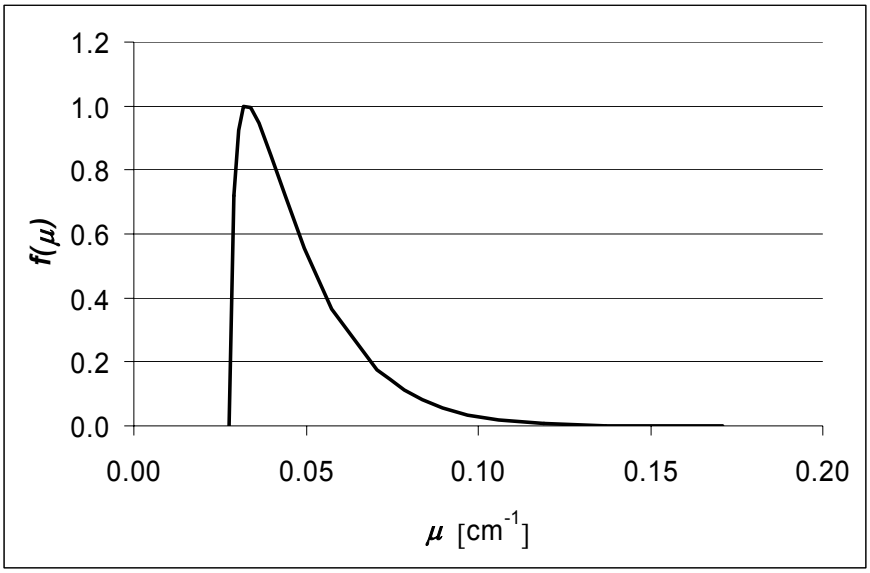

FIGURE 1. The spectral distribution $f(\mu)$, normalised to the maximum value, for a 6 MV open beam.

Since moments of higher order than two are very small for clinical spectra (this has been verified by numerical analyses using hypothetical clinical spectra), these moments will be difficult to resolve from transmission measurements due to statistical noise. This is supported by experimental observations by Bjärngard and Shackford [29] and Yu *et al.* [43]. Thus, Equation (5a) can be truncated into a second-order exponential, and the final expression for $T(z)$ is given by:

$$T(z) = \exp\left(-E[\mu]z + \frac{E[\mu^2] - E[\mu]^2}{2} z^2 \right) \qquad (5d)$$

The first moment, $E[\mu]$, is the average linear attenuation coefficient of $f(\mu)$, while the second moment, $E[\mu^2]$, includes information about the width of $f(\mu)$ [6]. The idea of using the width of the spectrum is not a novelty; Huang *et al.* [42] and Brahme and Andreo [44] have utilized this quantity to reconstruct spectra and to describe beam hardening, respectively. Both $E[\mu]$ and $E[\mu^2]$ can be obtained by fitting Equation (5d) to measured transmission data "free in air" using a mini-phantom. Although not recommended in

[6] By definition, $E[\mu^2]=Var(\mu)+E[\mu]^2$, where $Var(\mu)$ is the variance of the spectral distribution $f(\mu)$.

practice, $E[\mu]$ and $E[\mu^2]$ can also be derived from datasets of TPR (tissue-phantom ratios) [32]. Numerically, $E[\mu]$ is equal to the dose-weighted average attenuation coefficients used by other authors [29, 31]. The truncation of Equation (5a) into a second-order exponential (Equation (5d)) implies that only estimates of the true moments will be derived from transmission measurements. Numerical analyses have verified, however, that these estimates closely match the true values, which means that the unique correspondence between a measured transmission curve and the underlying spectrum is restricted to the first two moments – a conclusion which is generally valid.

2.2 A new beam quality specifier

An optimal beam quality specifier for clinical high-energy photon beams should be both simple to measure and work satisfactorily over the entire range of energies and accelerators used in radiotherapy. The most fundamental measure is the complete spectral distribution of primary photons, from which any dosimetric quantity can be determined. Unfortunately, complete knowledge of the spectral distribution is not attainable, either by using direct measurements or Monte Carlo simulations, or reconstruction from transmission measurements, as pointed out in the previous section. The determination of many dosimetric quantities, however, does not require complete knowledge of the spectral distribution, and accordingly, simplifications of the actual spectral shape can readily be made. For instance, there is no unique correspondence between the spectral distribution and depth-dose data; different spectra (with the same average energy) can result in similar depth-dose curves that agree with measured data within the uncertainty of these measurements [45]. Another example is the determination of Spencer-Attix restricted stopping power ratios (water-to-air), $s_{w,air}$, where most dosimetry protocols use a ratio of doses to determine $s_{w,air}$, e.g. tissue phantom ratios at 20 and 10 cm depth (TPR(20/10)) [5, 41], and percentage depth-dose at 10 cm depth $(\%dd(10)_x)$ in a clean photon beam [24][7]. This latter course of action has been found to be quite successful in terms of choosing $s_{w,air}$ under traditional reference conditions, i.e. on the central axis in open beams without external modulators (wedges, compensation filters, shadow trays for block support etc.). There are some uncertainties involved, however, in selecting correct values of $s_{w,air}$ in situations where the amount of filtration is varied (i.e. beam hardening or softening). For TPR(20/10), it has been shown that for photon beams with

[7] An overview of common photon beam quality specifiers used in radiotherapy dosimetry can be found in, for example, ICRU Report 64 [46].

the same value of TPR(20/10), but with a different amount of filtration, $s_{w,air}$ can differ by almost 1% [47-49]. Furthermore, some authors have reported that TPR(20/10) may be rather insensitive to changes in beam quality at higher energies [49, 50]. Although it is not optimal throughout the entire energy range of interest, Kosunen and Rogers [49] report that $\%dd(10)_x$ is more sensitive to beam quality changes. The determination of $\%dd(10)_x$, however, is affected by the level of contaminating electrons [51][8], which may limit the usefulness of this index [53]. In addition, neither TPR(20/10) nor $\%dd(10)_x$ is a practical index for use in describing the variation of beam quality with off-axis positions in the beam. Thus, neither of the two most commonly used beam quality specifiers completely fulfils the requirements on an optimal beam quality specifier.

It has also been proposed that the linear attenuation coefficient (μ) or the half-value layer (HVL) be used for beam quality specification [44, 54, 55]. Although easy to measure, an average μ (or HVL) suffers from the same limitations as TPR(20/10) in terms of predicting stopping power ratios for polyenergetic beams, especially when the beam is filtered. Nevertheless, the average μ can serve as an accurate beam quality specifier in many other situations, e.g. to determine the phantom scatter factor and TPR(20/10) [31, 32, 56, 57].

The first two moments of the spectral distribution ($E[\mu]$ and $E[\mu^2]$), on the other hand, possess some attractive features which make them better candidates for beam quality specification – they are easily measured using a simple narrow-beam technique and the effects of hardening or softening can be taken into account by the second moment $E[\mu^2]$.

In **Paper II**, thick-target bremsstrahlung spectra of different energies and with various degrees of filtration were generated as a common basis for an accurate determination of $s_{w,air}$, $E[\mu]$, and $E[\mu^2]$. Data for TPR(20/10) and $\%dd(10)_x$ were also generated in order to make an independent comparison of these beam quality specifiers, which are the subject of lively debate in the literature [49, 53, 58]. The combination of different energies and filters resulted in 60 different high-energy X-ray beams, which were used in an attempt to provide the full range of spectral shapes likely to be found across radiotherapy centres. In addition, a set of spectra[9] frequently referred to in the literature was included [49, 59].

---

[8] For high-energy beams (≥10 MV), contaminating electrons are removed by placing a 1 mm lead foil just below the accelerator head [51]. Measurements, i.e. $\%dd(10)_{Pb}$, are then related to $\%dd(10)_x$ by a relation given by Rogers and Yang [52].

[9] The following spectra were used: 4, 6, 10, 15, and 24 MV (Mohan), 10 and 20 MV (NRC), and 30 MV (Racetrack). These spectra can be found in the EGS4/DOSRZ software package distributed by NRC, Canada.

The following relationships between $s_{w,air}$ and TPR(20/10), $\%dd(10)_x$ and the first two moments were derived (see Figures 2-4 below):

$$s_{w,air} = A_1 - A_2 \cdot TPR(20/10) + A_3 \cdot TPR(20/10)^2 - A_4 \cdot TPR(20/10)^3 \quad (6a)$$

$$s_{w,air} = B_1 - B_2 \cdot \%dd(10)_x \quad (6b)$$

$$s_{w,air} = C_1 + C_2 \cdot E[\mu] - C_3 \cdot E[\mu]^2 + C_4 \cdot E[\mu]^3 - C_5 \cdot \frac{\sqrt{E[\mu^2] - E[\mu]^2}}{E[\mu]} \quad (6c)$$

The coefficients A_i, B_i and C_i are given in **Paper II** (Table 2). The last term in Equation (6c) is the relative standard deviation of $f(\mu)$, which is a measure of the width of the spectrum. This term is crucial for the relationship since it is affected by the filtration of the beam, as is demonstrated in Figure 5 in **Paper II**. The relationships given above for TPR(20/10) and $\%dd(10)_x$ closely match the data given by the IAEA [41] and the relation proposed by Rogers and Yang [52], respectively. To our knowledge, this is the first time the relation given by Rogers and Yang has been validated.

A more quantitative comparison between the different beam quality indices can be achieved by comparing the predicted (using the relationships in Equation (6)) and "true" (i.e. calculated directly from the spectra) $s_{w,air}$ values. This type of analysis clearly shows that the moments and $\%dd(10)_x$ are more accurate as beam quality specifiers than TPR(20/10) (Figures 6-8 and Table 3 in **Paper II**). This is true for both the thick-target spectra generated in **Paper II** and for the spectra generated by Mohan *et al.* [59] and Kosunen and Rogers [49]. Despite somewhat greater deviations at lower energies for $\%dd(10)_x$, there is no clear dependence on energy for any of the specifiers.

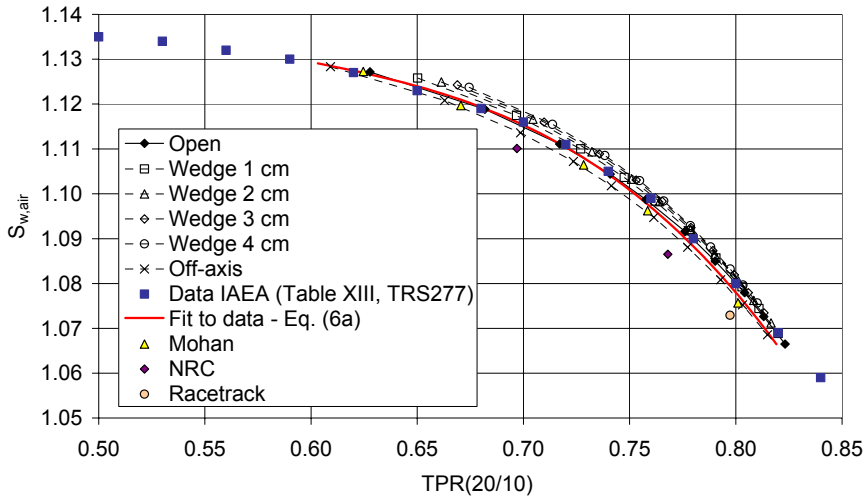

FIGURE 2. $s_{w,air}$ as a function of TPR(20/10) for the combination of spectra used in **Paper II**. The solid red line depicts the relationship given by Equation (6a). Data given by the IAEA [41] are included for comparison.

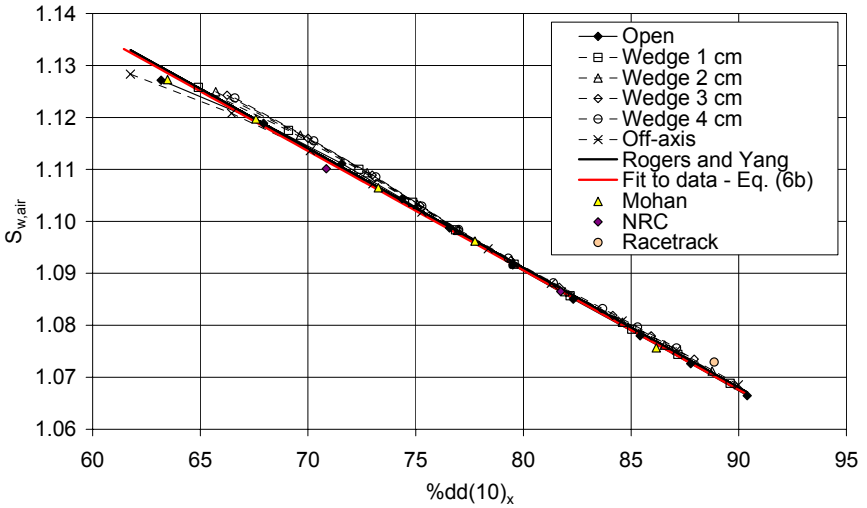

FIGURE 3. $s_{w,air}$ as a function of $\%dd(10)_x$ for the combination of spectra used in **Paper II**. The red line depicts the relationship given by Equation (6b). The relation given by Rogers and Yang [52] is included for comparison.

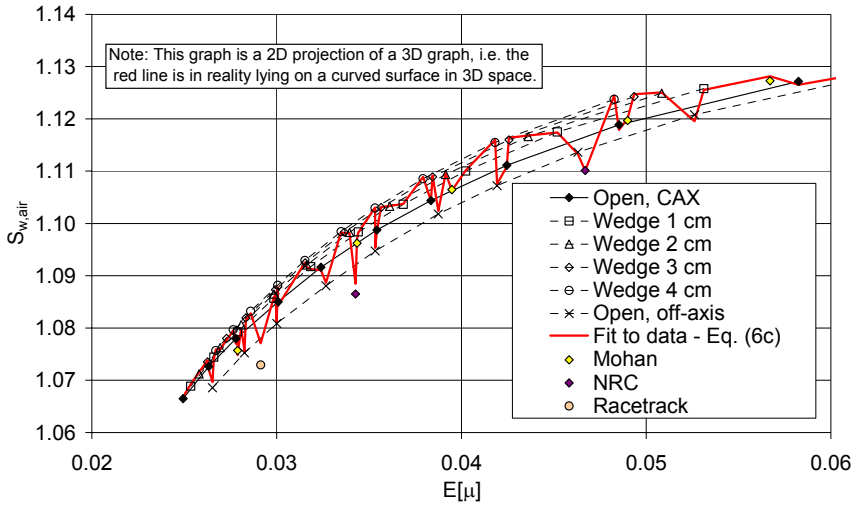

FIGURE 4. $s_{w,air}$ as a function of $E[\mu]$ and $E[\mu^2]$ for the combination of spectra used in **Paper II** (note that the graph does not include $E[\mu^2]$ since it is a 2D projection of a 3D graph). The red line depicts the relationship given by Equation (6c).

Given the results in **Paper II**, it is clear that the moments of the spectral distribution are highly suitable for the determination of stopping power ratios – they are more accurate than TPR(20/10) and the they are easier to measure than $\%dd(10)_x$. Once derived from narrow-beam measurements, the moments can also be used to calculate the transmission of the primary kerma (see above) and the scatter-to-primary kerma in the medium (see below). Thus, they certainly have the potential to be optimal beam quality specifiers for high-energy X-ray beams. It must be pointed out, however, that further work is required if the moments of the spectral distribution are to be recommended as beam quality indices for absolute ion chamber dosimetry. One must also bear in mind that, for the purpose of ion chamber dosimetry, the existing indices (i.e. TPR(20/10) and $\%dd(10)_x$) are well established throughout the radiotherapy community, and it is not likely that they will be replaced in the near future. Thus, the results presented in **Paper II** should not be interpreted as an attempt to replace TPR(20/10) or $\%dd(10)_x$ with a "better" index. By showing that the moments of the spectral distribution can be used for the accurate determination of a fundamental dosimetric quantity, the confidence in using these moments for other purposes (e.g. to determine the transmission factor and the scatter-to-primary kerma) is enhanced.

2.3 The scatter-to-primary kerma ratio

To determine the ratio between the scatter and primary kerma, the semi-empirical formalism proposed by Bjärngard and co-workers for the scatter-to-primary dose ratio is used [28, 30, 31]. When transient electronic equilibrium is established, this formalism can also be applied to the scatter-to-primary kerma ratio, i.e.:

$$\sigma(s,z) = \frac{a \cdot s \cdot z}{w \cdot s + z} \qquad (7)$$

The field size, s, is the side of the corresponding equivalent square field at depth z in the medium. For clinical beams, the parameters a and w are closely related to $E[\mu]$ [10] [30, 31, 60], according to:

$$a = E[\mu] \qquad [\text{cm}^{-1}] \qquad (8a)$$

$$w = 1.73 - 17.1E[\mu] \qquad (8b)$$

A tentative explanation of the equals sign between a and $E[\mu]$ in Equation (8a) is that when the predominant interaction in the medium is Compton scattering, each primary photon that interacts produces one scattered photon. The parameter w characterises the directional distribution of the scattered photons by weighting the relative importance of field size and depth in the denominator of Equation (7) [31]. Since $E[\mu]$ reflects the beam spectrum that determines the directional distribution of the scattered photons, a correlation between w and $E[\mu]$ seems reasonable. The derived linear relationship, however, must be regarded as a simplification unless confirmed by additional data [31]. Although not done in this work, a and w can also be derived from datasets of TPR or directly from the quality index TPR(20/10) according to Xiao *et al.* [32].

Thus, the only parameter needed to determine σ is $E[\mu]$, which is easily derived from narrow-beam measurements "free in air" using a mini-phantom. This simple semi-empirical formalism has proven to be accurate at depths below d_{max} [31, 56, 61]. At more shallow depths, however, the model is less accurate due to the approximations made in the derivation of σ (e.g. the number of backscattered photons is underestimated since $\sigma \to 0$ as $z \to 0$)

[10] For consistency, $E[\mu]$ is used instead of the dose-weighted average linear attenuation coefficient, μ, which is used by the authors cited. This has no implication whatsoever, since they are numerically equal.

[28], especially in low-energy beams with large field sizes. Fortunately, this is of minor importance for dose calculations at the prescription point, which should be positioned at depths well below the surface.

For rectangular and irregular fields (including fields shaped by multileaf collimators, MLCs), the concept of decomposing an arbitrary field of N vertices into 2N right triangles [62, 63] and differentiating Equation (7) into a pencil beam [33, 34] is used. The pencil beam is integrated over each right triangle and the sum of all integrations then yields σ. This method reduces the calculation time and is therefore well suited for implementation in a hand-held PC with limited processor speed.

2.4 The primary kerma "free in air"

The primary kerma "free in air" relative to a reference field is composed of three parts according to Equation (3); the head scatter *H(c)*, the inverse square law *I(f)* and the transmission factor of the shadow tray $k'_{o,t}(c)$.

The head-scatter, *H(c)*, is the variation in the primary kerma "free in air" at the isocentre with the collimator setting (*c*). In **Paper III**, *H(c)* was estimated with a ratio of polynomials fitted to measured data for square field sizes (normalised to *c*=10 cm), according to:

$$H(c) = \frac{a_1 + a_2 c}{1 + a_3 c + a_4 c^2} \qquad (9)$$

The coefficients a_n can be found in Table I in **Paper III**[11]. For rectangular fields, an equivalent collimator opening is used in order to take into account the collimator exchange effect [64-66]. This effect is described in more detail in **Paper III**. For irregular fields shaped with MLC, the same equivalent field size is used as in the calculation of σ. Head-scatter data are collected "free in air" with an ionisation chamber at the isocentre and a suitable build-up cap [67]. If the spectral distribution of the incident beam remains constant when the collimator setting is changed, measurements can also be done at 10 cm depth in a mini-phantom according to the recommendations given by ESTRO (see below) [4]. In **Paper III**, the model was shown to reproduce measurements to within ±0.5% (1 SD) (with an average deviation of less than 0.2%) for both square and rectangular fields.

[11] Note that the coefficients a_1, a_2, a_3, and a_4 are referred to as a, b, c, and d, respectively, in Table I in **Paper III**.

The inverse square law, $I(f)$, is given by the square of the ratio f_{ref}/f, where f is the distance between the source and the calculation point and f_{ref} is the reference distance (100 cm).

The transmission factor of the shadow tray, $k'_{o,t}(c)$, is a correction factor for the attenuation of the primary kerma in the shadow tray which supports the blocks. It is defined as the ratio of the doses measured "free in air" under reference conditions and for the collimator opening used for the treatment, with and without the shadow tray, for the same number of monitor units [4]. It varies with beam quality and depends slightly on the collimator opening because of the additional photons scattered by the shadow tray. There is no variation with SSD, however. More details about this correction factor can be found in ESTRO Booklet No. 3 [4]. In this work, individual factors were used for beams with the same nominal accelerating potential (i.e. the same factor was used for both open and wedged beams), while possible variations with collimator setting were neglected.

2.5 Heterogeneities

Heterogeneities in the patient are accounted for by replacing the physical depth with the radiological depth in the expression for the transmission of the primary kerma in the patient (i.e. Equation (5d)). Only bulk densities are used for lung (0.3 g/cm^3) and bone (1.2 g/cm^3). In practice, the distance the beam passes through lung and/or bone is estimated from the CT-based anatomical cross-section through the calculation point.

2.6 Wedges

Currently, accelerators from Varian and Elekta/Philips are supported and this section has therefore been divided into physical wedges (Elekta/Philips) and dynamic wedges (Varian).

Physical wedges

Elekta/Philips accelerators use an internal motorized physical wedge which is mounted between the ionisation chambers and the upper pair of collimators. With this construction, any wedge angle between 0 and 60° can be produced by combining wedged and non-wedged beams. In this work, the wedged beam is treated as a separate beam quality with its own datasets, including the dose per monitor unit in the reference geometry, the relative primary kerma in air (i.e. head-scatter factors), and the beam quality specifiers (i.e.

the moments of the spectral distribution), which in turn are used to determine $T(z)$ and σ.

Dynamic wedges

Varian accelerators use an enhanced dynamic wedge (EDW) to generate a wedged beam. This type of wedge is more difficult to control, but it is has the advantage of a constant energy distribution over the field. This means that the beam quality will not change for a wedged field in comparison to a non-wedged field as is the case for physical wedges. The wedge is generated by moving one of the collimators during irradiation according to the fractional exposure concept [68, 69], which has been adopted for the EDW [70]. The number of monitor units required to deliver a wedged field is given by multiplying the number of monitor units for the open field by a wedge factor (WF). This wedge factor is equal to the ratio between the number of monitor units delivered when the moving collimator passes the central axis (or the fan line through the point of calculation) and the final number of monitor units. This ratio can be estimated from the segmented treatment table (STT) supplied by the vendor (for more details, see **Paper III**).

2.7 Comparisons with measurements

Using the formalism presented above, the percentage depth-dose (PDD) value along the central axis of the beam is given by:

$$PDD(z) = 100 \frac{f_{ref}^2}{f^2} \frac{T(z)}{T_{ref}} \frac{(1+\sigma)}{(1+\sigma_{ref})} \quad [\%], \qquad (10)$$

In **Paper III**, calculated percentage depth-dose curves (using Equation 10) were compared with measurements for square fields. When shallow depths (down to 5 cm) were excluded, the average difference was found to be less than 0.3%, and the standard deviation for all energies (4, 6, 10 and 18 MV) was 0.9%.

2.8 The electron disequilibrium factor

As mentioned above, the calculation model has been found accurate as long as calculations are made at depths where transient equilibrium exists. This is true as long as the model is used to check the absorbed dose at the prescription point, which should be in a region without steep dose gradients, and preferably close to the centre of the planning target volume [6, 39, 40]. It would be favourable, however, to have a model which can be used to

calculate the dose also at the nominal depth of dose maximum (d_{max}) (the dose at d_{max} is hereafter called "entrance dose"). Entrance doses are needed since they are compared with *in vivo* measurements, using diodes or TLDs (thermo-luminescent dosimeters) positioned on the patient's skin. In Sweden, *in vivo* dosimetry is required by law, and entrance dose measurements are mandatory at least once in every beam portal[12]. At d_{max}, however, the assumption of transient electronic equilibrium is not valid, and calculations may deviate by as much as 6-7%. In addition, at lower energies (4-6 MV), the expression for the scatter-to-primary kerma in Equation (7) underestimates the number of backscattered photons at shallow depths (i.e. $\sigma \rightarrow 0$ as $z \rightarrow 0$).

The state of electronic equilibrium at d_{max} is determined by many factors. It is often convenient to divide the electron fluence at d_{max} into two parts:

1. Secondary electrons generated by photon interactions in the irradiated medium. This effect has been studied by e.g. Bjärngard *et al.* [71], Loevinger [35] and Nizin [72].
2. Electrons produced in the air or in the structures of the accelerator head. There are numerous studies in the literature involving the effect of these so-called contaminating electrons at the surface of a phantom/patient [73-81]. Although not as frequent as studies of the surface dose, several studies can be found on the effects of contaminating electrons at depths around d_{max} [73, 78, 79, 81-85].

In **Paper IV**, a method is proposed in which the effects mentioned above are taken into account. An "entrance dose factor" (EDF) is defined to correct the original calculations at d_{max}. The EDF is given by the ratio of the measured and calculated percentage depth dose values at d_{max}, according to:

$$EDF = \frac{PDD(d_{\max})_{measured}}{PDD(d_{\max})_{calculated}} \qquad (11)$$

Calculated percentage depth dose values are given by Equation (10).

The results in **Paper IV** show that there is a variation in EDF with field size (c) and beam quality ($E[\mu]$), while no obvious trend can be found with varying SSD (80-100 cm) or with the presence/absence of an acrylic shadow tray (used for block support) in the beam. Since there are no other known studies employing the same approach as that described in **Paper IV**, it is impossible to quantitatively compare the results with those from other

[12] The Swedish Radiation Protection Authority's Regulations (SSI FS 2000:4) on Radiation Therapy (http://www.ssi.se/forfattning/PDF_Eng/2000-4e.PDF)

studies. A qualitative comparison with numerous studies on the effect of contaminating electrons is, however, possible, if one assumes that the amount of secondary electrons generated by photon interactions in the irradiated medium does not change with field size (a valid assumption if lateral electronic equilibrium is established), SSD or the presence of a shadow tray in the beam, and that the influence of backscattered photons at d_{max} is minimal. In that case, the variation in EDF with the parameters mentioned is mainly due to a varying amount of contaminating electrons at d_{max}.

Regarding the effect of varying the SSD, a review of the literature shows that the relative amount of contaminating electrons at the surface or in the build-up region has been found to either increase [74, 79, 80, 86-88] or remain constant [80-82, 89, 90] when SSD is decreased from 100 to 80 cm. The latter corresponds to the results in **Paper IV**. Thus, it seems likely that the decrease in the production of contaminating electrons in air with a decreasing SSD is counteracted by an increasing contribution from contaminating electrons generated in the accelerator head.

Regarding the effect of an acrylic shadow tray in the beam, most studies report a clear effect at the surface when inserting a tray into the beam [74-76, 80-82, 86, 87, 90, 91]. This effect is limited (or even non-existent), however, at depths around nominal d_{max} [81, 82, 86, 90], which supports the findings in **Paper IV**. A possible explanation could be that electrons generated in the tray have a dominant low-energy component or a wide angular spread, which means that they do not reach the depth of dose maximum.

The field size dependence is illustrated in Figure 5, where EDF values for each beam quality are plotted as a function of field size. The shape of the field size dependence is similar for each beam quality, and a third-order polynomial can be fitted to all the data (after each dataset has been normalised to c=20 cm):

$$EDF(c) = 1.53\times10^{-6}c^3 - 1.53\times10^{-4}c^2 + 5.24\times10^{-3}c + 0.944 \qquad (12)$$

There can be no physical interpretation of the shape of this relationship, as contaminating electrons are generated both in the treatment head and in the intervening air gap, and the variation with field size is accordingly rather complex. It should also be pointed out that the shape of the field size dependence in Equation (12) is valid only at d_{max}. At other depths (e.g. at the surface), the results may be quite different. Several investigations have been performed on this subject and they all show an increasing contribution with field size, although the shape of this variation may vary [71, 73-76, 80-82, 86-89, 91-93].

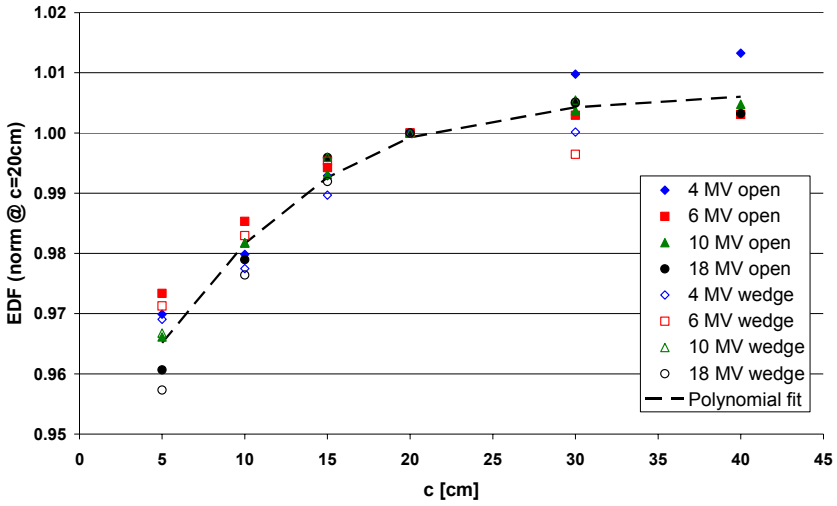

FIGURE 5. The entrance dose factor (EDF) as a function of field size. Data for each beam quality are averaged values with and without a tray, for SSD=80, 90, and 100 cm. Each dataset has been normalised to c=20 cm, and the dashed line represents the polynomial fit given by Equation (12).

A simple linear relationship between the absolute levels of EDF at c=20 cm (i.e. $EDF_{c=20}$) and the beam quality specifier, $E[\mu]$, was also derived in **Paper IV** (see Figure 6 below):

$$EDF_{c=20}\left(E[\mu]\right) = 1.50E[\mu] + 0.957 \qquad (13)$$

A physical explanation of Equation (13) is not trivial since both phantom-generated electrons and contaminating electrons contribute to the variation in $EDF_{c=20}$ with beam quality. Regarding the contaminating electrons, which are generated upstream mainly by primary photons, an increase in proportion to the interaction probability, $E[\mu]$, (which has a similar energy dependency for all relevant materials), should be expected. However, a similar, simple prediction regarding the phantom-generated electrons is not possible, and the combined effect remains to be investigated.

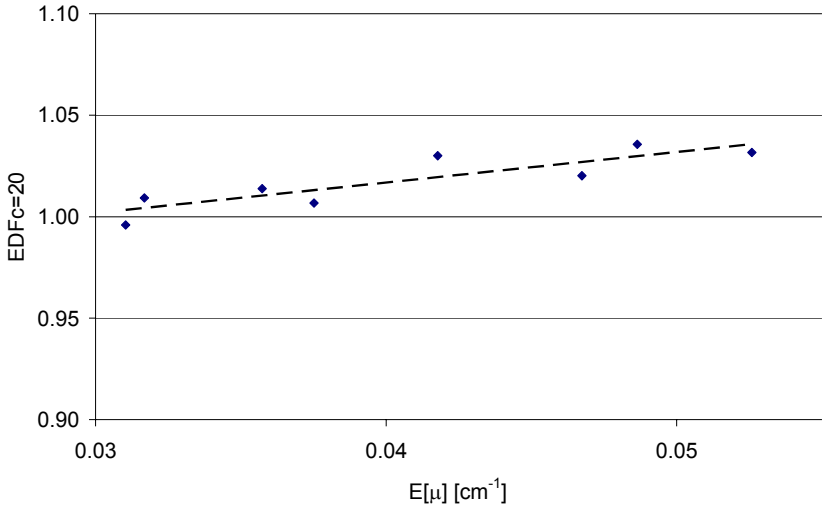

FIGURE 6. The variation of the entrance dose factor at c=20 cm ($EDF_{c=20}$) with the beam quality parameter $E[\mu]$. The dashed line represents the fit given by Equation (13).

Assuming that the variation of EDF with field size is independent of the variation with beam quality, the resulting entrance dose factor can be written as:

$$EDF(c, E[\mu]) = EDF(c) \cdot EDF_{c=20}(E[\mu]) \qquad (14)$$

Figure 7 shows a histogram of the percentage deviations between calculated (using the entrance dose factor) and measured percentage depth-dose values at d_{max}. The deviations are within 1.7% (2 SD), but can be further reduced if "true" values of $EDF_{c=20}$ are used instead of Equation (13)[13]. Doses at d_{max} are then predicted with an accuracy of 1.2% (2 SD). Although somewhat less accurate, the first approach is more attractive since it better fits into the original version of the calculation model.

An attractive feature of the presented formalism is that no extra parameters or measurements are needed in order to implement the entrance dose factor in the calculation model ($E[\mu]$ is already measured). It should to be remembered, however, that Equations (12-14) can only be used in

[13] In practice, the only measurement needed to derive "true" values of $EDF_{c=20}$ is a single, relative measurement at d_{max} with SSD=100 cm, c=20 cm, and with no tray present. Generally, this dataset is already available and no extra measurements are thus required.

combination with the algorithms of the original calculation model, and they are only valid at the nominal depth of dose maximum. A more general description of EDF (i.e. including the depth dependence) would require division of the electron fluence into two parts as described above [71, 81]. This approach, however, leads to rather complicated relationships, far from the simple and accurate equations derived here.

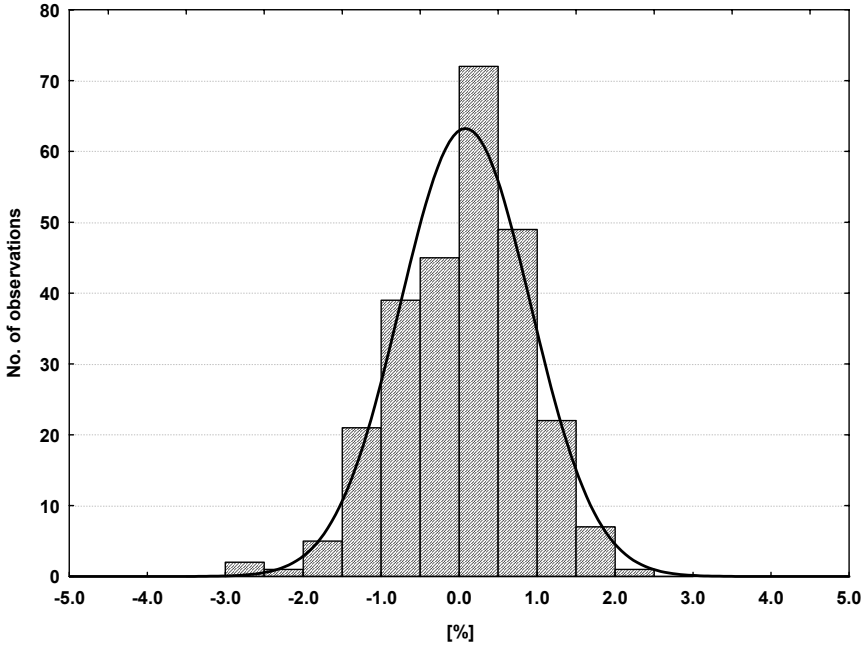

FIGURE 7. A histogram showing the percentage deviations between calculated (using the entrance dose factor given by Equations (12-14)) and measured percentage depth-dose values at d_{max}. The maximum, average and standard deviations are 2.70%, 0.06% and 0.86%, respectively. The solid line represents a normal distribution with an average value of 0.06% and a standard error of 0.86%.

The results in **Paper IV** were originally derived for accelerators from Philips/Elekta. Although the contribution of contaminating electrons at the surface may vary between different accelerator manufactures [88], the field size dependence at d_{max} may be similar for other accelerators. As a test of this hypothesis, percentage depth-dose values derived from measurements on two Varian accelerators (Clinac 600C - 4 MV & Clinac 2100C - 6 and 18 MV[14]) were compared with calculations using Equations (12-14). Good agreement was found; doses at d_{max} were predicted to within 2% (2 SD). Future studies will show if this is also the case for accelerators from other manufactures.

[14] Data from the University Hospital in Malmö, Sweden.

It is worth noting that the investigation in **Paper IV** did not include the effect of electron disequilibrium on blocked or MLC-shaped fields (only square fields were studied). While the effect of blocks is believed to be of minor importance at d_{max} [81, 82], further studies should be performed to determine possible effects caused by elongated and MLC-shaped fields.

2.9 Concluding remarks about the calculation model

With the addition of a correction factor for the entrance dose, the calculation model now forms a complete tool to check the absorbed dose to the patient, both at the prescription point and at d_{max}. The complete set of algorithms forming the basis for an independent calculation system will hereafter be referred to as "HandCalc". Combining the uncertainties of the head-scatter model and the percentage depth-dose calculations, gives a total uncertainty in HandCalc for standard beam geometries of 1.0% (1 SD) at depths greater than 5 cm. At d_{max}, the accuracy is 0.9% (1 SD). Thus, one of the overall objectives defined in the introduction has been achieved. It should be emphasized, however, that this level of accuracy is only valid for rectangular fields impinging on a cubic water phantom. To evaluate HandCalc in more complex beam geometries, a comparison with a 3D treatment planning system is required. This comparison is presented in **Paper III** and will be described in detail below. Although not done in this work, another solution would be to compare HandCalc with, for example, TLD measurements in an anthropomorphic phantom. Note that the present version of HandCalc only supports calculations on the central axis. A method of including off-axis calculations will be described at the end of this thesis.

It is clear that the most important parameter in HandCalc is the first moment of the spectral distribution, i.e. $E[\mu]$. This parameter is used in the determination of the transmission factor (in combination with the second moment, $E[\mu^2]$), the scatter-to-primary kerma ratio and the entrance dose factor. Although not used explicitly in HandCalc, $E[\mu]$ and $E[\mu^2]$ can also be used to determine stopping-power ratios. Thus, the moments of the spectral distribution serve well for specification of the beam quality. The usefulness of $E[\mu]$ alone as a beam quality specifier has also been acknowledged by, for example, Bjärngard and Vadash [56], who used the dose-weighted average attenuation coefficient for beam quality specification (which is numerically equal to $E[\mu]$). Thus, accurate determination of $E[\mu]$ and $E[\mu^2]$ is crucial for HandCalc to function properly. This will be dealt with in the following section.

3. IN-AIR EQUIVALENT MEASUREMENTS

Several of the parameters in the calculation model are derived from relative measurements which are stated to be "free in air". It is becoming increasingly more common to use a mini-phantom to perform these types of measurements [38, 57, 94-96], and in a publication from ESTRO [4], recommendations on using a mini-phantom for relative in-air measurements in megavoltage X-ray beams are given (e.g. for output ratios, volume scatter factors, wedge factors and transmission tray factors). The mini-phantom should resemble water (e.g. PMMA or polystyrene), and have a square or cylindrical cross-section perpendicular to its axis. Due to the presence of contaminating electrons, the depth of measurement should be 10 cm, and in order to achieve lateral electronic equilibrium, the diameter should be at least 4 cm. High-Z materials are discussed briefly, but are not recommended for extensive use. A small cylindrical ionisation chamber is recommended as a detector, but other studies have verified that diodes may also be used for e.g. output measurements in air [97, 98]. The versatility of the ESTRO mini-phantom has been studied in detail by Georg and Dutreix [57], especially for measurements in wedged beams and at off-axis positions. In the present work, measurements "free in air" with a mini-phantom were required to derive the moments of the spectral distribution (i.e. $E[\mu]$ and $E[\mu^2]$), the head scatter and the transmission factor of the shadow tray.

The phrase "free in air" must be interpreted as a measurement at a point in free air, without any influence from the surrounding medium. While this has an obvious meaning for radiometric quantities, it needs to be further exploited for dosimetric quantities[15]. In particular, dose measurements inside a mini-phantom will always depend on both the material and size of the phantom. While effects due to the choice of material are not considered in this work, effects due to the size of the mini-phantom are dealt with by using the novel concept of "in-air equivalence". Accordingly, relative measurements with a mini-phantom are said to be in-air equivalent if dose ratios equal primary kerma ratios in water at a point in free air, which has a strict physical meaning [100].

The difference between the dose measured in a mini-phantom and the primary kerma at a point in free air is due to the attenuation of primary photons, the production and transport of scattered photons, and, although of minor importance, the transport of secondary and contaminating electrons and bremsstrahlung losses. Fortunately, in certain relative measurements with a mini-phantom, the incident spectrum is fairly constant (e.g. output measurement in air), and these effects cancel (i.e. the conditions for in-air equivalence are fulfilled). In other situations, however, the spectral

[15] For a definition of radiometric and dosimetric quantities, see e.g. ICRU 33 [99].

distribution may change considerably, and measurements with a mini-phantom may no longer be in-air equivalent.

In an earlier study, the effects of beam softening at off-axis positions were investigated, and the results clearly show that both the attenuation of primary photons and the production of scattered photons inside a mini-phantom vary considerably when the shape of the spectrum changes [101]. In this particular case, however, the decrease in primary photons inside the mini-phantom was found to be almost fully compensated for by a corresponding increase in scattered photons, and the net effect on the absorbed dose at the point of measurement was found to be minimal (less than 1%). Thus, it was concluded that primary off-axis ratios can be deduced directly from in-air equivalent measurements using a mini-phantom. This conclusion, however, is strictly valid only for mini-phantoms where the depth of measurement is 5 cm. For the ESTRO mini-phantom (with a 10 cm depth of measurement), preliminary calculations show that the net effect is greater than 2%[16], which indicates that measurements are not in-air equivalent.

In **Paper I**, a field of application for the mini-phantom which is not addressed by ESTRO was investigated – transmission measurements in narrow-beam geometry. In this work, transmission measurements of the primary kerma are required in order to derive the moments of the spectral distribution. Increasing interest in these types of measurements can also be found in the literature, often in the context of beam quality specifications [29, 43, 55, 57]. Inevitably, this is a measurement setup wherein large spectral shifts take place (beam hardening) due to the absorber (often water) interposed between the mini-phantom and the X-ray source. An example of this spectral shift is given in Figure 8. Since beam hardening will give rise to a variation in both the attenuation of primary photons and the production of scattered photons inside the mini-phantom, measurements may no longer be in-air equivalent. Concern associated with beam hardening in measurements of the primary kerma has also been addressed by Iwasaki [102], who concluded that the primary water kerma for a 10 MV photon beam can be measured using a build-up cap of low-Z material. The theoretical work by Iwasaki, however, only covered build-up caps, while the investigation in **Paper I** included mini-phantoms of larger dimensions and 4 different energies (4, 6, 10 and 18 MV).

[16] Numerical analyses with the ESTRO mini-phantom at 12.5 cm from the central axis show that the net effects are 1.8% (6 MV) and 2.4% (18 MV). At 10 cm from the central axis, the net effect is 1.1% (25 MV).

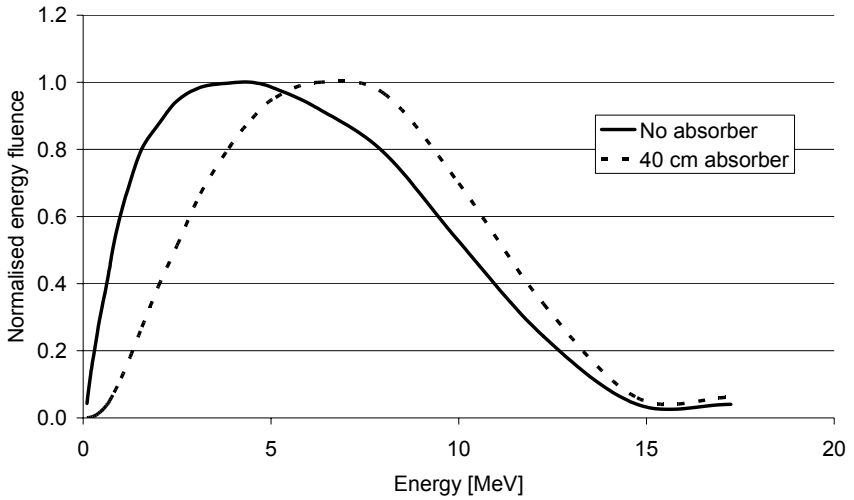

FIGURE 8. The normalised energy fluence (normalised to the maximum value) as a function of energy for an 18 MV beam (spectra from the TPS). The solid and dashed lines represent the spectral distributions before and after passing through 40 cm of water (representing a commonly used absorber thickness), respectively. The beam-hardening effect is caused by a higher interaction probability in water of photons with lower energies compared with photons with higher energies.

In **Paper I**, absorbed dose and primary kerma were scored as a function of depth in a cylindrical mini-phantom (made of water) for 4, 6, 10 and 18 MV beams using the Monte Carlo code EGS4 [103]. The narrow-beam geometry is illustrated in Figure 1 in **Paper I**. While scored values of dose reflect real measurements in the mini-phantom, the primary kerma in free air is given by extrapolation of the primary kerma back to zero depth in the mini-phantom, i.e. at the surface of the mini-phantom. The degree of in-air equivalence is then determined from the quotient of the ratio of the dose in water (with and without the absorber present) and the ratio of the primary kerma in air (with and without the absorber present), according to:

$$c_x(z) = \left(\frac{D_x(z)}{D_0(z)}\right)_{water} \Bigg/ \left(\frac{K_{P,x}}{K_{P,0}}\right)_{in-air} \qquad (15)$$

In the equation above, the subscript "x" denotes the absorber thickness (20 and 40 cm) and the index "0" indicates no absorber. Note that the dose ratios are given as a function of the depth, z, in the mini-phantom, while the primary kerma ratios are defined at the surface of the mini-phantom. Thus,

whenever measurements with a mini-phantom are in-air equivalent, $c_x(z)$ should equal unity.

The results given in **Paper I** clearly show that transmission measurements at 10 cm depth in a mini-phantom are not in-air equivalent. The largest deviation (7%) can be found at 4 MV, with an absorber thickness of 40 cm. This is illustrated in Figure 9 below (similar graphs for 6, 10 and 18 MV can be found in **Paper I**). A change in the balance between attenuation and scattering inside the mini-phantom can explain these results. When the beam is hardened, the amount of primary photons will increase and the generation of scattered photons will decrease at the point of measurement inside the mini-phantom. Although these two effects act in opposite directions (with respect to dose deposition at the point of measurement), the net effect does not cancel at 10 cm depth; the increase in primary photons is too large to be counterbalanced by the decrease in scatter production. Although the results indicate greater deviation at 4 MV, there is no clear dependence on energy. The greater deviations at 4 MV are expected, however, since hardening has a considerable influence on low-energy beams. At higher energies, however, this effect is counteracted by beam softening caused by pair production.

In Table 1, the range of depths in which $c_x(z)$ equals unity to within 1% is given for all energies included in the investigation and for absorber thicknesses of 20 and 40 cm. It is clear that depths somewhat greater than the depth of dose maximum are required for in-air equivalence, and this is where the detector should be positioned in the mini-phantom. This is according to expectations, since a spectral change will have less effect on scatter and attenuation closer to the surface. It is also worth noting that the results at 10 MV are in accordance with the results presented by Iwasaki [102]. It may be argued that contaminating electrons may influence the measurements if the detector is positioned closer than 10 cm to the surface of the mini-phantom. With the present narrow-beam geometry (i.e. a long distance and a small field size), however, disturbances from contaminating electrons should be minimal, even at depths close to the depth of dose maximum [81].

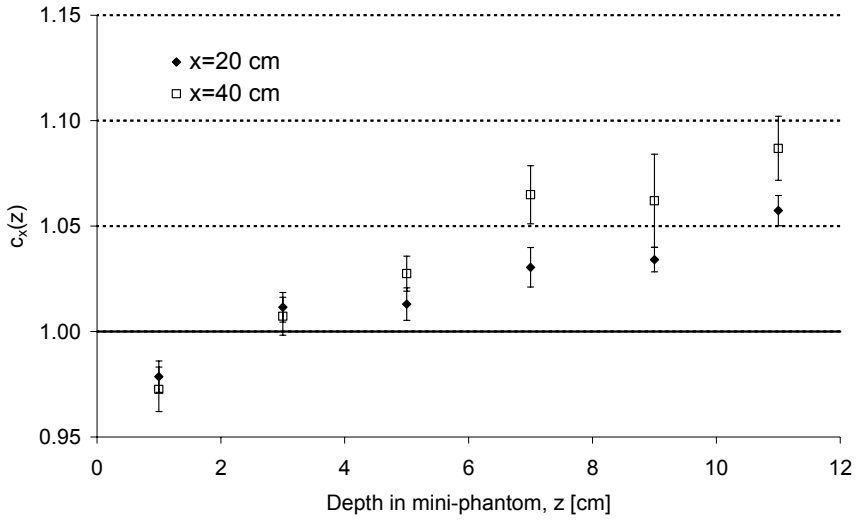

FIGURE 9. The variation of $c_x(z)$ with depth z in a mini-phantom. Data are for a 4 MV beam, with water absorber thicknesses of 20 cm (♦) and 40 cm (□). The error bars represent 1 SD.

TABLE 1. $c_x(z)$ at 10 cm depth in a mini-phantom (column 3), and the interval in which $c_x(z)$ is within 1% of unity (column 4). Results are given for 4, 6, 10 and 18 MV, with absorber thicknesses of 20 and 40 cm.

Energy [MV]	Absorber thickness x [cm]	c_x(z=10 cm)	Depths at which $0.99 < c_x < 1.01$ [cm]
4	20	1.046	1.7-2.9
	40	1.079	2.0-3.3
6	20	1.025	2.5-5.7
	40	1.032	2.6-4.9
10	20	1.022	2.6-6.7
	40	1.050	2.7-3.7
18	20	1.023	3.3-4.8
	40	1.032	3.9-4.9

4. IMPLEMENTATION AND EVALUATION

4.1 The Personal Digital Assistant (PDA)

The rapid development in computer technology during recent decades has had considerable influence on the field of radiotherapy. Computed tomography, Monte Carlo systems, dose planning algorithms and IMRT (intensity modulated radiotherapy) are only a few examples where modern computers are a prerequisite for efficient work. In the continuing development of faster and smaller computers, one of the latest trends is the Personal Digital Assistant (PDA) – a hand-held PC, the size of a palm. The manufacturers of PDAs are making continuous developments, and today the machines come equipped with powerful processors, distinct colour screens, large memory capacities, efficient batteries and advanced software. Together with its small size, these performance characteristics have made the PDA an optimal platform for HandCalc. Once HandCalc is implemented in a PDA, fast and accurate calculations can be made bedside during the first treatment session in order to reveal both systematic and random errors in patient dosimetry.

Several different models of PDAs have been tested and evaluated during the past few years and at present, PDAs with the Microsoft™ Pocket PC operating system are being used. A picture of a PDA manufactured by Compaq is shown in Figure 10. The user interface is intuitive and familiar to the regular PC-user, and consequently, a minimum of extra training is needed in order to operate the PDA. The small size makes the PDA extremely portable and it can be used for several days before it has to be recharged. Synchronization with a desktop PC is achieved by a USB cradle or a wireless network. During this synchronization, field parameters can be downloaded directly from the R&V system (Helax-Visir, MDS Nordion) to speed up the input of data. It may be argued that this option invalidates the independence of the calculations, but since the R&V system controls the accelerator, it is actually better to use these downloaded parameters than to manually enter the parameters from e.g. the treatment chart.

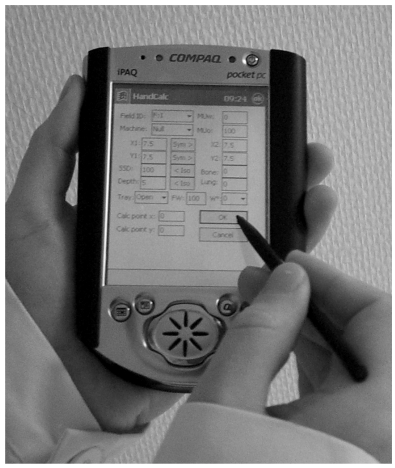

FIGURE 10. Photograph of a Compaq PDA (iPAQ 3630).

4.2 The software HandCalc

The entire set of equations in HandCalc has been programmed into the PDA using the programming language C++. The software is intuitive and easy to use and input is entered with a stylus or by using built-in, drop-down menus (Figure 10). Screen dumps from the software showing the modes of operation are presented in Figure 11. The current version supports linear accelerators from Varian and Elekta/Philips, and all data are stored in a database which is easily updated or revised by an authorized user. With the calculation model presented above, only nine parameters are needed per beam quality (note that wedges are treated as separate qualities). These parameters can be summarized as follows.

- One factor describing the dose per monitor unit in a reference situation
- The first two moments of the spectral distribution
- Four parameters describing the variation of the primary kerma in air with collimator opening, i.e. head scatter (preliminary data indicate, however, that even fewer parameters can be used to describe the head-scatter variation)
- One factor describing the collimator exchange effect[17]
- The transmission factor of the shadow tray

An example of the data required at the radiation therapy department at Lund University Hospital is given in Table 1 in **Paper III**. As mentioned earlier, the version of HandCalc which has been used clinically in this work does not support entrance or off-axis dose calculations. Including entrance dose calculations would not require any extra parameters, while the number of additional parameters for off-axis calculations remains to be investigated.

Note also that the name of the independent calculation software in **Paper III** is "MUcalc", while HandCalc is used throughout this thesis and in **Papers IV** and **V**. MUcalc and HandCalc are in fact two different software applications, and there are substantial differences in terms of the user interface. While MUcalc was written and compiled for PDAs based on the EPOC32 operating system with larger screens and built-in keyboards, HandCalc has been compiled for PDAs based on the Pocket PC operating system with smaller screens and without a built-in keyboard. In terms of differences in the calculation model, the only difference which may have an impact on the dose calculations is the determination of the equivalent field size for irregular fields. While MUcalc used a method in which the percentage blocked area was estimated manually, HandCalc uses a pencil-beam approach to calculate the equivalent field size [33, 62, 63]. In most

[17] For more details on this factor, see **Paper III.**

cases, however, this will not have any influence on the final result. With the introduction of HandCalc it also became possible to download treatment parameters and field shapes (i.e. blocks and MLC) from the R&V system and to use the graphical interface in order to change the field shape directly on the screen.

FIGURE 11. *(next two pages)* Screen dumps showing the workflow of HandCalc software when calculating the dose to the prescription point. To start with, the user can choose either to download treatment data from the R&V system in order to speed up the input of data, or to enter all data manually (**A**). The *treatment summary screen* (**B**) contains information about treatment site, dose per fraction and the number of fractions. It is also possible to perform simple BED (biological equivalent dose) calculations. If the user has chosen to download parameters from the R&V system, field identification, machine (including energy), monitor units (open/wedge), field size (X1,X2,Y1,Y2), and wedge angle (only for Varian machines)) are already given on the *field parameter screen* (**C**), while SSD and the depth to the prescription point have to be entered manually. Corrections for heterogeneities are made (note that it is only the primary kerma which is corrected) by entering the amount of lung and/or bone in front of the calculation point. This amount is estimated from the CT-based anatomical cross-section through the calculation point. Corrections for block trays can also be included by choosing a single or double shadow tray. The field shape can be edited either manually (**D**) or with an automatic method in which a certain percentage of the field is blocked out using a pre-defined shape (**E**). It is also possible to download the actual field shape (including both blocks and MLC) from the R&V system (**F**). The equivalent square field size at the depth of calculation is also presented. On the *dose summary screen* (**G**), the calculated absorbed dose to the prescription point is presented for each field together with the total dose. If the deviation between the calculated and prescribed dose is greater than the action level (±4%), the total dose will be shown in red (otherwise in green). Entrance doses (FD) are also given for each field, but the user has to be careful with these figures since the entrance dose factor has not yet been included in HandCalc. The final screen dump shows the *report screen* (**H**), where the explanation of a deviation can be entered. It is also possible to indicate if a recalculation has been performed. The information on this screen, together with information about the percentage deviation, treatment site, machine, and energy, are then saved in a log file for later analysis.

A

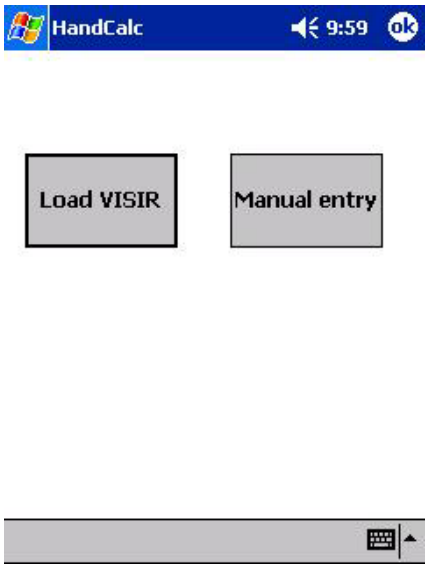
HandCalc
9:59
Load VISIR
Manual entry

B

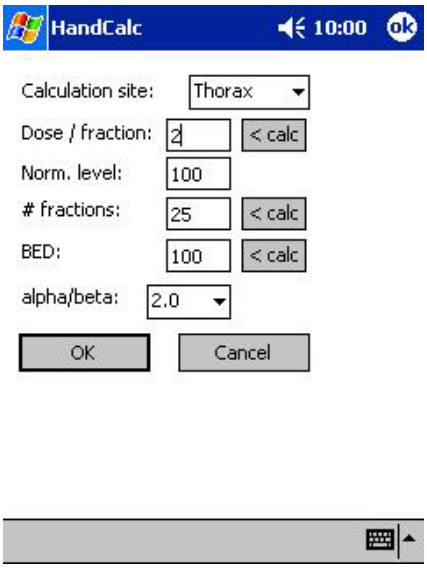
HandCalc
10:00
Calculation site:
Thorax
Dose / fraction:
2
< calc
Norm. level:
100
fractions:
25
< calc
BED:
100
< calc
alpha/beta:
2.0
OK
Cancel

C

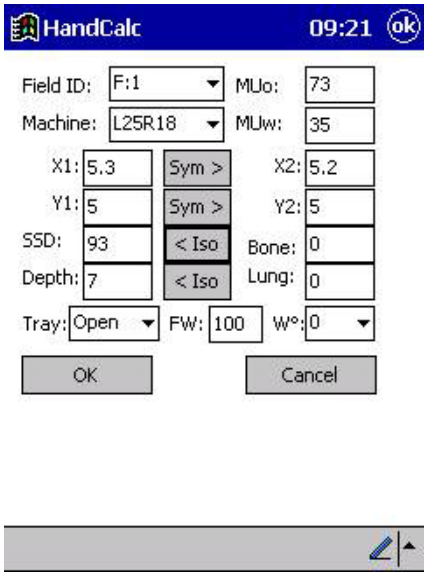
HandCalc
09:21
Field ID:
F:1
MUo:
73
Machine:
L25R18
MUw:
35
X1:
5.3
Sym >
X2:
5.2
Y1:
5
Sym >
Y2:
5
SSD:
93
< Iso
Bone:
0
Depth:
7
< Iso
Lung:
0
Tray:
Open
FW:
100
W°:
0
OK
Cancel

D

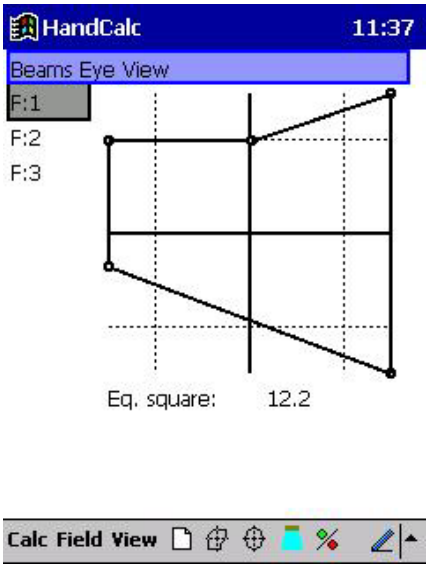
HandCalc
11:37
Beams Eye View
F:1
F:2
F:3
Eq. square:
12.2
Calc Field View

E

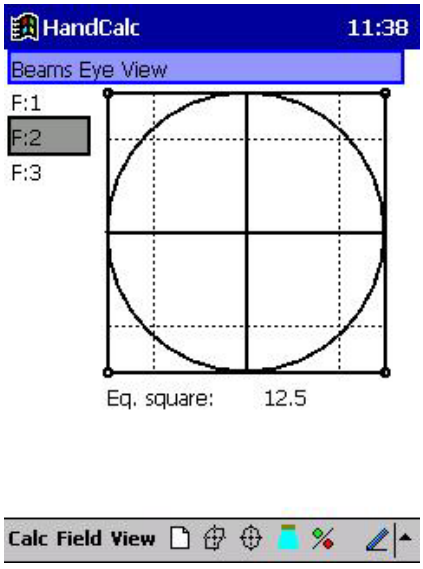
HandCalc
11:38
Beams Eye View
F:1
F:2
F:3
Eq. square: 12.5
Calc Field View

F

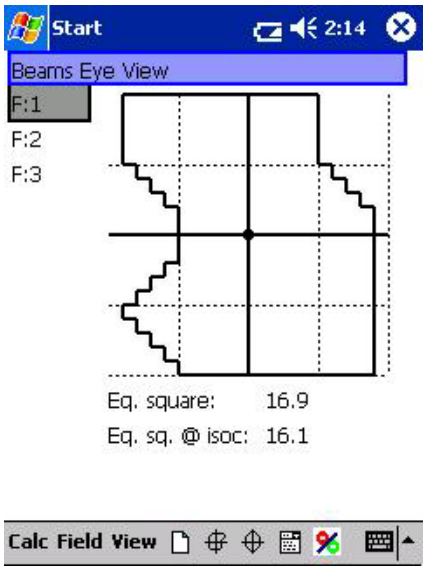
Start
2:14
Beams Eye View
F:1
F:2
F:3
Eq. square: 16.9
Eq. sq. @ isoc: 16.1
Calc Field View

G

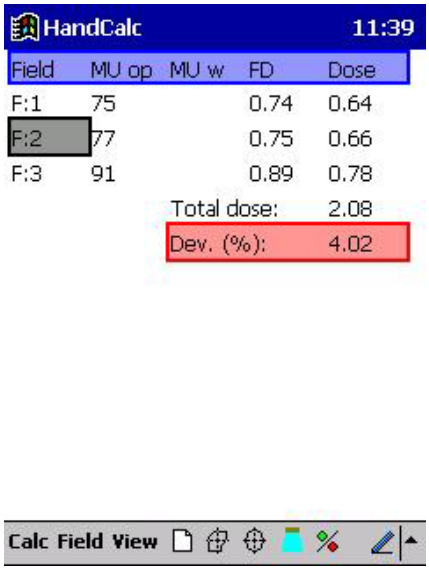
HandCalc
11:39
Field MU op MU w FD Dose
F:1 75 0.74 0.64
F:2 77 0.75 0.66
F:3 91 0.89 0.78
Total dose: 2.08
Dev. (%): 4.02
Calc Field View

H

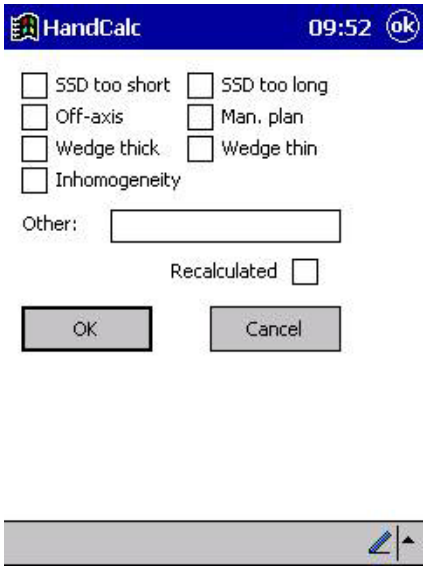
HandCalc
09:52
ok
SSD too short
SSD too long
Off-axis
Man. plan
Wedge thick
Wedge thin
Inhomogeneity
Other:
Recalculated
OK
Cancel

4.3 Derivation of an action level for HandCalc

In **Paper III**, a comparison with a state-of-the-art treatment planning system (Helax-TMS, MDS Nordion) was performed to determine an action level for HandCalc. This action level must be set such that when HandCalc reports a deviation outside this level, one can conclude, with a certain statistical significance, that an error is present in the patient dataset. The monitor units determined by the TPS for a certain prescription dose were entered into HandCalc together with all other necessary parameters for 117 patients with a total of 552 treatment fields. All patients had a computerized 3D dose plan and they represented various treatment techniques and sites commonly used in the clinic.

The Helax-TMS models primary and head-scatter fluence from the accelerator and convolves these fluences with a machine-specific pencil beam to obtain the dose distribution. It also calculates the number of monitor units required to deliver the prescribed dose to the prescription point. The system has been extensively described and verified in several papers [104-111], and the accuracy is considered to be around 2% (1 SD).

The evaluation in **Paper III** shows no specific trend with treatment site and the distribution of deviations between HandCalc and the TPS is presented in Figure 12. This distribution is somewhat skewed towards the negative side, and deviations range from –5.6 to +4.8% with an average of –0.17%[18]. Assuming a normal distribution[19], the standard deviation (SD) was found to be ±2.05%. For the clinical situation, when using HandCalc as an independent check of the TPS calculation, the action level was set to ±4% (1.96 SD). A "consequential deviation" (i.e. a deviation greater than the action level, which forces the user to take some kind of action) will therefore occur in 5% of the cases, even if there are no real errors present. It was also argued, that if there are errors in the patient dataset, a consequential deviation will occur with high probability. With the results in **Paper III**, the second overall objective laid out in the introduction, concerning the accuracy of the calculation model, has been fulfilled.

---

[18] Note that an error during the preparation of **Paper III** resulted in different values for the average deviation in the abstract, results and conclusion sections of **Paper III**. The correct value is -0.17%, which is the value given in the results section of **Paper III** and in this thesis.

[19] Unfortunately, the number of patients included in this study was somewhat too small to draw any reliable conclusions about the shape of the distribution. Considering that HandCalc and the TPS are completely independent of each other and assuming that there are no systematic deviations which include all treatment geometries in either system, the normal distribution was assumed to be the most likely.

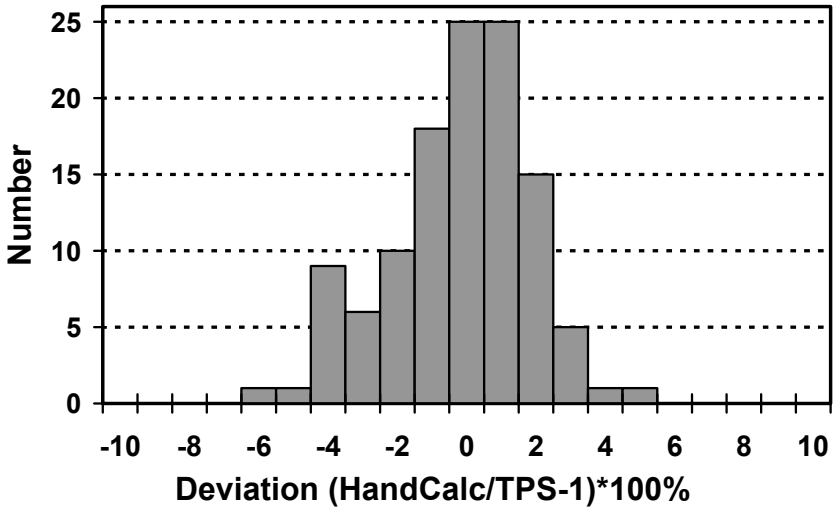

FIGURE 12. A histogram showing the percentage deviations between HandCalc (note that the name "MUcalc" is used in **Paper III**) and the TPS. The deviation was calculated as (HandCalc/TPS-1) and is given in percent. (Each bin is one unit wide and the label indicates the centre of the bin.)

4.4 Clinical evaluation

HandCalc, implemented in a PDA, has been used by several different users (mainly physicists) in routine clinical work at the Radiation Therapy Department at Lund University Hospital (Sweden). Since HandCalc has been implemented as a standard windows application on the PDA, very little training was required before a new user could start using the system. An important feature of HandCalc is the built-in report function (Figure 11), with which data can be saved in a log file for later evaluation. This log file includes information on treatment site, beam energy, treatment unit, and the deviation between the calculated and prescribed dose, for example. Data for almost 700 patients have been logged during a period of about one year in order to investigate consequential deviations (i.e. those outside the action level) occurring in a large sample of patients during routine clinical work.

The results of this evaluation (including 693 patients) are presented in **Paper V** and in Tables 2 and 3 below. The data in Table 2 include patients for whom the dose and monitor units have been calculated using either manual methods (i.e. manual plans[20]) (176 cases) or the TPS (517 cases).

[20] In manual plans, the absorbed dose and the monitor units are calculated by manual interpolation in data tables of depth-dose and output ratio.

Data from patients with TPS plans have also been further divided into different treatment sites. The evaluation with respect to different energies and accelerators is closely linked to the evaluation of the treatment sites and is therefore not shown explicitly. It is clearly demonstrated that HandCalc is very accurate for manual plans (average deviation, 0.05%). This is expected since these plans are often rather "simple" (i.e. nearly rectangular field shapes with, in general, no correction for heterogeneities) and the calculated dose is more or less a direct comparison with standard measurements in a cubic water phantom. In view of this, the results agree well with the results in **Paper III** (see Section 2.8), where HandCalc was shown to reproduce measurements to within 1% (the standard deviation for manual plans in this evaluation is 0.9%). Since the accuracy of HandCalc is much better when used in these simpler cases than in more complex situations (i.e. TPS plans where 1 SD=2.05%), it was argued in **Paper V** that a separate action level of ±1.8% (1.96 SD) should be used for manual plans instead of using a common action level of ±4% for all plans.

The only treatment site where HandCalc overestimates the dose (i.e. in comparison to the TPS) is in the thorax (average deviation, 0.7%), where the calculation point is situated close to (or inside) a heterogeneity (i.e. the lung). Since HandCalc only corrects the primary kerma and not the scatter kerma, this deviation is expected. For many other treatment sites, there is a substantial negative deviation between HandCalc and the TPS, which will be explained below.

In Table 3, all consequential deviations for TPS plans are summarized. A consequential deviation was observed in 8.7% of the cases and a closer examination (using the log report in HandCalc) shows that they can be divided into "false" (4.8%) and "true" (3.9%) deviations. False consequential deviations, which means that no error was found in the patient dataset, are due to limitations in HandCalc (e.g. situations where the calculation point is situated behind bone or lung, or close to the surface/contour of the patient). Due to the criteria used in the derivation of the action level, 5% of the cases are expected to be false deviations, which is close to the level found in this study (4.8%). This indicates that the action level derived in **Paper III** works satisfactorily also when used on a larger sample of TPS plans.

TABLE 2. Deviations between calculations using HandCalc and calculations using the TPS ("TPS plans") or manual methods ("manual plans"). The TPS plans have also been further divided into different treatment sites. The figures within parentheses in column five denote one standard deviation [%]. The last two columns present the number of calculations for which the deviation is outside the action level (±4%) and above ±5%. The figures within parentheses in these last two columns are the number of false deviations.

Treatment site	Patients	Min [%]	Max [%]	Average [%]	Median [%]	≥±4%	≥±5%
Manual plans	176	-3.6	3.6	0.05 (0.9)	0.1	0 (0)	0 (0)
All TPS plans	517	-6.9	6.8	-0.8 (2.4)	-0.9	45 (25)	20 (11)
Brain	*35*	*-6.5*	*4.1*	*-0.7 (2.3)*	*-0.9*	*3 (1)*	*1 (1)*
Gynaecologic	*24*	*-6.4*	*5.7*	*-2.2 (2.3)*	*-2.3*	*4 (1)*	*2 (1)*
Head & Neck	*63*	*-6.9*	*4.7*	*-1.3 (2.7)*	*-1.6*	*8 (5)*	*4 (1)*
Tangential breast	*121*	*-5.0*	*4.4*	*-0.6 (2.0)*	*-0.6*	*5 (4)*	*0 (0)*
Other	*30*	*-3.8*	*3.8*	*-0.3 (2.1)*	*-0.1*	*0 (0)*	*0 (0)*
Pelvis	*184*	*-5.8*	*5.4*	*-1.0 (2.2)*	*-1.2*	*15 (5)*	*6 (2)*
Thorax	*60*	*-5.7*	*6.8*	*0.7 (2.9)*	*0.8*	*10 (9)*	*7 (6)*
Total	**693**	**-6.9**	**6.8**	**-0.5 (2.2)**	**-0.35**	**45 (25)**	**20 (11)**

TABLE 3. The number of patients with TPS plans where the deviation between HandCalc and the TPS plan is greater than 4% and 5%. Deviations are divided into false and true. The numbers within parentheses correspond to the percentage of the total number of patients with TPS plans (i.e. 517).

Type of deviation	≥ ±4%	≥ ±5%
False (limitations in HandCalc)	25 (4.8%)	9 (1.7%)
True	20 (3.9%)	11 (2.1%)
Total	**45 (8.7%)**	**20 (3.9%)**

True consequential deviations, on the other hand, imply that there are errors in the patient dataset which may jeopardise the clinical outcome of the treatment. In this study, true deviations are found only in TPS plans and they are due, in all cases, to a systematic deviation in the SSD for patients treated mainly in the pelvic area. For these patients, the SSD used by the TPS during planning is larger than the actual SSD measured on the patient at the time of the first treatment. This means that the dose (to the prescription point) calculated by the TPS will be too high, which explains the shift of the average deviations in Table 2 towards the negative side for many treatment sites. A thorough investigation was performed in order to find the underlying reason for this systematic deviation, and it seems to be related to the old type of CT used during the major part of this study[21]. Although this type of deviation can be observed if the actual SSD is checked prior to the first treatment, HandCalc adds another dimension since it calculates the absorbed dose to the prescription point from each and every field. Thus, the decision as to whether a correction has to be applied or not is better supported.

Tables 2 and 3 also include statistics for deviations greater than ±5%, which normally corresponds to the required accuracy in delivered dose [6, 20]. The percentage found in this work (2.1%) is somewhat higher than those presented by Calandrino (0.75% and 1.3%) [15, 16] and Williams (0.5%) [14], but considerably lower than those reported by ICRU (Report 24) in 1976 [6]. In the latter case, it is believed that the introduction of R&V systems has had a positive effect on the number of errors.

The automatic downloading of field parameters from the R&V system to HandCalc makes the system very fast and reliable. In many cases, only the SSD and the depth to the prescription point have to be entered manually, and the time required to perform an independent calculation with HandCalc is estimated to be, on average, less than two minutes for a standard plan. If a consequential deviation is found, an investigation has to be performed in order to reveal if this is a true or false deviation before treatment can continue. If it is a false deviation (e.g. thorax treatment with heterogeneities) it is normally found within a minute and the treatment can continue without any changes. If it is a true deviation, however, a recalculation should be carried out before the treatment can continue.

Since HandCalc has been used in addition to existing quality control routines in the department, the results from the analysis described above can also be used as an indirect measure of the reliability of these routines. Except for the systematic deviations in SSD, no other true deviations have been

[21] The problems have more or less disappeared with the installation of a new CT scanner.

identified during this study. This demonstrates that the extensive checks and analyses performed prior to the clinical use of each newly introduced system in the treatment chain (e.g. CT scanner, TPS, simulators, R&V system, and treatment units) and inter-system tests of data transfer between these individual systems have been successful. It also shows that the existing quality control routines with double manual checks of e.g. treatment charts, MU calculations and R&V system, minimize the number of unnoticed errors in the treatment chain.

4.5 Other applications

Besides HandCalc, several other clinical applications have been developed and implemented in a PDA. One of them is the personal agenda, where personalized schedules for each physicist on clinical duty are presented. These schedules are downloaded from the booking module of the R&V system and they contain information about patients on the treatment, simulator, CT and fixation units. In addition, most parts of Microsoft Outlook are available in the PDA, including e-mails, contacts, tasks and notes. Internet and intranet pages can be viewed either on-line using equipment for wireless communication (i.e. WLAN), or off-line when information has been downloaded to the PDA for later viewing. Special pages for the intra- and Internet have been developed in order to take full advantage of the small screen of the PDA. One of these pages is a clinical handbook with interactive memos for the medical physicist, containing information about different treatment regimens, treatment units, etc. Another in-house-developed application is MU calculation software for electron beams.

5. CONCLUDING REMARKS & FUTURE PERSPECTIVES

The overall objective of this work has been achieved, i.e. to develop, implement and evaluate an accurate independent system with which to calculate the absorbed dose to the prescription point and the depth of dose maximum. The calculation system is based on models originally derived by Bjärngard and co-workers [28-31] requiring only a limited amount of extra measurements to be made in order to derive the necessary parameters. It can be used in rather complex beam geometries, and it has been found to be accurate to within 1% (1 SD) and 2% (1 SD) when compared with standard measurements and a TPS, respectively.

In **Paper II**, it was shown that the transmission of the primary kerma in water can be described by an exponential, where the coefficients are uniquely

given by the first two moments of the spectral distribution. The first moment of the spectral distribution also enters into the expressions for the scatter kerma and the entrance dose factor. To further enhance confidence in the use of the moments for beam quality specification, a comparison with other beam quality indices, in terms of predicting stopping power ratios, was made. The results of this comparison clearly show that the first two moments of the spectral distribution are suitable for beam quality specification over the entire range of energies and accelerators used in radiotherapy.

A thorough investigation on how to best measure the moments of the spectral distribution was undertaken and is presented in **Paper I**. In this particular work, in-air equivalent measurements using a mini-phantom were defined, and it was concluded that the mini-phantom recommended by ESTRO (i.e. with a measurement depth of 10 cm) was not an optimal tool with which to measure the moments of the spectral distribution. Instead, measurements should be carried out at depths somewhat greater than the depth of dose maximum. In the future, it would be interesting to (re-)examine the degree of in-air equivalence in off-axis [101] and head-scatter measurements with the ESTRO mini-phantom using the same method as in **Paper I**.

In **Paper IV**, the calculation model was improved in order to account for the effect of electron disequilibrium at the depth of dose maximum. This was done by introducing an entrance dose factor, which was shown to be independent of the SSD and the presence of a shadow tray (for block support) in the beam. Variations with field size and beam quality (i.e. the first moment of the spectral distribution) were detected, however, and appropriate formulae to take these variations into account were derived. The entrance dose factor will be implemented in the next version of the calculation system. Since the study described in **Paper IV** only included Elekta/Philips and Varian accelerators and square fields, further studies are required in order to confirm the validity of the model for other manufactures and for irregular field shapes. Monte Carlo simulations, including the full geometry of the accelerator head and the intervening air gap, may then prove to be an important tool in studying, for example, the complicated behaviour of contaminating electrons [33, 78, 79, 84, 85, 112].

By comparing the calculation model with calculations using a commercial TPS, an action level of ±4% was chosen (**Paper III**). It must be pointed out, however, that this action level is only strictly valid for the TPS used in this study (i.e. Helax-TMS, MDS Nordion). Further studies are needed before it can be applied to other TPS systems. All parts of the calculation model (except the entrance dose factor) were compiled into a software application (HandCalc) which was implemented in a hand-held PC (PDA).

HandCalc has been tested on almost 700 patients (**Paper V**), and the results indicate that separate action levels should be used – one for manual plans (±1.8%) and one for 3D computerized plans (±4.0%). A thorough investigation of deviations greater than the action level (referred to as "consequential deviations") revealed that these deviations can be either true or false. False deviations are due to limitations in HandCalc, while true deviations imply that there are errors in the patient dataset which may jeopardise the clinical outcome of the treatment. The investigation described in **Paper V** showed that true deviations were solely due to a systematic deviation in SSD in 3D computerized plans for patients treated mainly in the pelvic area.

The absence of any other systematic errors indicates that the current level of checks and analyses performed prior to the clinical use of each newly introduced system is adequate. The absence of random errors shows that the current routines involving double manual checks of the treatment chart, MU calculations and R&V system etc., minimize the number of unnoticed errors in the treatment chain. With the introduction of HandCalc, some of these manual checks may be replaced. It may also be argued that HandCalc can partly replace *in vivo* dosimetry since verification of the position of the patient is accomplished within the system (the actual SSD has to be entered in HandCalc). *In vivo* dosimetry can never be fully replaced, however, since it detects errors which are not detected with HandCalc or any other method (e.g. machine malfunction). Today, it is common practice to measure the entrance dose with diodes upon administering the first two fractions and to perform occasional checks of the SSD during the remaining course of the treatment.

With future versions of HandCalc (including e.g. entrance dose calculations), it will also be possible to use the system for "primary" monitor unit calculations for patients not undergoing 3D dose planning (i.e. manual plans). This will make calculations more effective since field parameters and field shapes can be downloaded from the R&V system. Moreover, calculations will probably be less subject to human errors. With this approach, however, another independent calculation system has to be used to check the calculations at the treatment unit.

By implementing HandCalc in a PDA, the user is provided with a fast and accurate tool to check the dose with an independent method while the patient is set up for the first treatment. Due to the simple and intuitive user interface, only a limited amount of initial training is required before a new user can start using HandCalc. The method is more powerful than simple manual checks since HandCalc can be used in complex beam geometries (including heterogeneities and irregular field shapes). It should be pointed out, however, that the current version of HandCalc only supports

calculations with high-energy X-rays and cases in which the calculation point is on the central axis. In practice, this means that many cases where asymmetrical fields are used (e.g. in head and neck treatments) are excluded. To include off-axis calculations, changes in beam quality and primary kerma "free in air" with off-axis positions would have to be determined. Including changes in beam quality (i.e. the moments of the spectral distribution) in the calculation model is straightforward. The variation of beam quality with off-axis distance can either be derived from separate transmission measurements in narrow-beam geometry or by using a generic expression [113]. Including changes in the primary kerma "free in air" in the calculation model is, however, not so trivial. One possible solution is to use the head-scatter expression derived in this work in combination with a primary off-axis factor [101]. While this approach may be rather accurate for open beams, it will probably not work for wedged beams (i.e. physical wedges). Thus, further investigations are required before off-axis calculations can be implemented in HandCalc.

The differences between the formalisms used in this work and in the work by ESTRO [4, 21] are not that substantial. Both formalisms utilize measurements in a mini-phantom, but since the ESTRO formalism also requires measurements in a large water phantom, it is more labour intensive with respect to the initial data acquisition. With HandCalc, only 9 parameters are needed (see Section 4.2) and these are derived from absolute dosimetry measurements in water, head-scatter measurements in air, transmission measurements in air with and without the shadow tray, and transmission measurements in air in narrow-beam geometry. In most clinics, several of these measurements will already have been done during commissioning of the treatment unit, and usually only the narrow-beam measurements remain to be executed (which take less than one hour on a dual-energy machine). Apart from a difference in the number of extra measurements, the two formalisms differ in the calculation of the dose from scattered photons in the patient and in the handling of wedges. Regarding scattered dose, the model proposed by Bjärngard and co-workers is more flexible since it can be differentiated and used in pencil-beam calculations (especially useful in complex beam geometries) [33, 34]. Regarding wedges, the ESTRO formalism treats these as a modification of an open beam, while wedges are treated as separate beam qualities (with their own set of data) in the formalism presented in this work. Both formalisms have to be improved, however, before they can accurately calculate doses at off-axis positions [26, 27]. A combination of the two formalisms may be the optimal solution for the best calculation system in the future, including support, for example, for IMRT.

The PDA has proven to be a versatile platform on which many different applications can be used together in an interactive and user-friendly way (see Section 4.5). The most obvious advantage of implementing software on a PDA in comparison with a stationary PC is its portability. This advantage is more apparent in large institutions with many accelerators and at satellite clinics employing consultant physicists/doctors. Instead of installing many stationary PCs throughout the department, one PDA can be used at all locations. Ideally, all applications should be accessible from any type of client, and the user should be able to choose the preferred device. For this reason, a project has been initiated of which the aim is to convert all local applications on the PDA into standard web applications, accessible, in principle, from any available computer, stationary or mobile. These web applications should also be better integrated with the R&V system in order to be able to access relevant patient information at any time or place.

ACKNOWLEDGEMENTS

Many people have contributed to the completion of this thesis and I would like to express my deepest gratitude to the following people for their scientific guidance, technical assistance during measurements, skilful manufacturing of equipment, proofreading of manuscripts, IT knowledge, guidance in mathematics and statistics, inspiration, personal support, friendship and love:

Bertil Persson, Crister Ceberg and his wife Jeanette, Per Nilsson, Tommy Knöös, Inger-Lena Lamm, Michael Ljungberg, Bengt Bjärngard, Andrej Tomaszewicz, Kerstin Löfvander-Thapper, Per Wendel, Roland Perfekt, Tobias Rydén, Per-Anders Ivert, Per Munck af Rosenschöld, Peter Björk, Elinore Wieslander, Katarina Sjögreen, Kurt Larsson, Lars Andersson-Ljus, Sven Bäck, Anna Karlsson, Michael Garkavij, Gudrun Svahn-Tapper, Inger Erlandsson, Ann Findlater-Jonasson, Helen Sheppard, Camilla Borrebaeck, Dennis Stråhed, Anders Toryd, Thomas Hjerpe, staff at the departments of Radiation Physics and Radiation Therapy in Lund, my parents, my brother and sisters, and finally my wife Anette.

I would also like to thank the following for financial support:

- The Swedish Cancer Society
- The Royal Physiographic Society in Lund (Academy for the Natural Sciences, Medicine and Technology)
- The Knowledge Foundation - the programme for IT in healthcare
- Research funds from Lund University Hospital.

REFERENCES

1. Brahme A. Dosimetric precision requirements in radiation therapy. *Acta Radiol Oncol*. 1984; **23**: 379-391.
2. Brahme A, Chavaudra J, Landberg T, McCullough EC, Nusslin F, Rawlinson JA, Svensson G, Svensson H. Accuracy requirements and quality assurance of external beam therapy with photons and electrons. *Acta Oncol* Suppl. 1. 1988.
3. Dische S, Saunders MI, Williams C, Hopkins A, Aird E. Precision in reporting the dose given in a course of radiotherapy. *Radiother Oncol*. 1993; **29**: 287-293.
4. Dutreix A, Bjärngard BE, Bridier A, Mijnheer B, Shaw JE, Svensson H. Physics for clinical radiotherapy - Monitor unit calculation for high energy photon beams. ESTRO Booklet No. 3. Leuven-Apeldoorn: Garant; 1997.
5. IAEA International Atomic Energy Agency. Absorbed dose determination in external beam radiotherapy: An international code of practice for dosimetry based on standards for absorbed dose to water. IAEA Technical Reports Series No. 398. Vienna: IAEA; 2000.
6. ICRU International Commission on Radiation Units and Measurements. Determination of absorbed dose in a patient irradiated by beams of X or gamma rays in radiotherapy procedures. ICRU Report 24. Bethesda, MD: ICRU; 1976.
7. Mijnheer BJ, Battermann JJ, Wambersie A. What degree of accuracy is required and can be achieved in photon and neutron therapy? *Radiother Oncol*. 1987; **8**: 237-252.
8. Mijnheer BJ, Battermann JJ, Wambersie A. Reply to: Precision and accuracy in radiotherapy. *Radiother Oncol*. 1989; **14**: 163-167.
9. Valli MC, Prina M, Bossi A, Cazzaniga LF, Cosentino D, Scandolaro L, Ostinelli A, Monti A, Cappelletti P. Evaluation of most frequent errors in daily compilation and use of a radiation treatment chart. *Radiother Oncol*. 1994; **32**: 87-89.
10. Leunens G, Verstraete J, Van den Bogaert W, Van Dam J, Dutreix A, van der Schueren E. Human errors in data transfer during the preparation and delivery of radiation treatment affecting the final result: "garbage in, garbage out". *Radiother Oncol*. 1992; **23**: 217-222.
11. Verstraete J, Huyskens DP. Use of QA forms to register procedural errors in a radiotherapy department in an attempt to improve the overall process: A pilot study. *Journal of Radiotherapy in Practice*. 2002; **3**.

12. Bate MT, Speleers B, Vakaet LAML, De Neve WJ. Quality control and error detection in the radiotherapy treatment process. *Journal of Radiotherapy in Practice*. 1999; **1**: 125-134.
13. Swann-D'Emilia B, Chu JC, Daywalt J. Misadministration of prescribed radiation dose. *Med Dosim*. 1990; **15**: 185-191.
14. Williams JR, Bradnam MS, McCurrach GM, Deehan C, Johnston S. A system for the quality audit of treatment dose delivery in radiotherapy. *Radiother Oncol*. 1991; **20**: 197-202.
15. Calandrino R, Cattaneo GM, Del Vecchio A, Fiorino C, Longobardi B, Signorotto P. Human errors in the calculation of monitor units in clinical radiotherapy practice. *Radiother Oncol*. 1993; **28**: 86-88.
16. Calandrino R, Cattaneo GM, Fiorino C, Longobardi B, Mangili P, Signorotto P. Detection of systematic errors in external radiotherapy before treatment delivery. *Radiother Oncol*. 1997; **45**: 271-274.
17. Duggan L, Kron T, Howlett S, Skov A, O'Brien P. An independent check of treatment plan, prescription and dose calculation as a QA procedure. *Radiother Oncol*. 1997; **42**: 297-301.
18. Hill RF, Perez MD, Beckham WA. An independent check method of radiotherapy computer plan derived monitor units. *Australas Phys Eng Sci Med*. 1998; **21**: 79-84.
19. Fraass B, Doppke K, Hunt M, Kutcher G, Starkschall G, Stern R, Van Dyke J. AAPM Radiation Therapy Committee Task Group 53: Quality assurance for clinical radiotherapy treatment planning. *Med Phys*. 1998; **25**: 1773-1829.
20. Kutcher GJ, Coia L, Gillin M, Hanson WF, Leibel S, Morton RJ, Palta JR, Purdy JA, Reinstein LE, Svensson GK, *et al*. Comprehensive QA for radiation oncology: report of AAPM Radiation Therapy Committee Task Group 40. *Med Phys*. 1994; **21**: 581-618.
21. Mijnheer B, Bridier A, Garibaldi K, Torzsok K, Venselaar J. Physics for clinical radiotherapy - Monitor unit calculation for high energy photon beams - Practical examples.. ESTRO Booklet No. 6. Brussels: ESTRO; 2001.
22. Andreo P. Uncertainties in dosimetric data and beam calibration. *Int J Radiat Oncol Biol Phys*. 1990; **19**: 1233-1247.
23. Ahnesjö A, Aspradakis MM. Dose calculations for external photon beams in radiotherapy. *Phys Med Biol*. 1999; **44**: R99-155.
24. Almond PR, Biggs PJ, Coursey BM, Hanson WF, Huq MS, Nath R, Rogers DWO. AAPM's TG-51 protocol for clinical reference dosimetry of high-energy photon and electron beams. *Med Phys*. 1999; **26**: 1847-1870.

25. Leszczynski KW, Dunscombe PB. Independent corroboration of monitor unit calculations performed by a 3D computerized planning system. *Journal of Applied Clinical Medical Physics*. 2000; **1**: 120-125.
26. Georg D. Monitor unit calculation on the beam axis of open and wedged asymmetric high-energy photon beams. *Phys Med Biol*. 1999; **44**: 2987-3007.
27. Smulders B, Bruinvis IA, Mijnheer BJ. Monitor unit calculations for wedged asymmetric photon beams. *Phys Med Biol*. 2002; **47**: 2013-2030.
28. Bjärngard BE, Petti PL. Description of the scatter component in photon-beam data. *Phys Med Biol*. 1988; **33**: 21-32.
29. Bjärngard BE, Shackford H. Attenuation in high-energy x-ray beams. *Med Phys*. 1994; **21**: 1069-1073.
30. Bjärngard BE, Vadash P. Analysis of central-axis doses for high-energy x rays. *Med Phys*. 1995; **22**: 1191-1195.
31. Bjärngard BE, Vadash P, Ceberg CP. Quality control of measured x-ray beam data. *Med Phys*. 1997; **24**: 1441-1444.
32. Xiao Y, Altschuler MD, Bjärngard BE. Quality assurance of central axis dose data for photon beams by means of a functional representation of the tissue phantom ratio. *Phys Med Biol*. 1998; **43**: 2195-2206.
33. Ceberg CP, Bjärngard BE, Zhu TC. Experimental determination of the dose kernel in high-energy x-ray beams. *Med Phys*. 1996; **23**: 505-511.
34. Ceberg CP, Bjärngard BE. The effects of divergence and nonuniformity on the x-ray pencil-beam dose kernel. *Med Phys*. 1996; **23**: 1531-1535.
35. Loevinger R. A formalism for calculation of absorbed dose to a medium from photon and electron beams. *Med Phys*. 1981; **8**: 1-12.
36. Hannallah D, Zhu TC, Bjärngard BE. Electron disequilibrium in high-energy x-ray beams. *Med Phys*. 1996; **23**: 1867-1871.
37. Li XA, Soubra M, Szanto J, Gerig LH. Lateral electron equilibrium and electron contamination in measurements of head-scatter factors using miniphantoms and brass caps. *Med Phys*. 1995; **22**: 1167-1170.
38. Zefkili S, Kappas C, Rosenwald JC. On-axis and off-axis primary dose component in high energy photon beams. *Med Phys*. 1994; **21**: 799-808.
39. ICRU International Commission on Radiation Units and Measurements. Prescribing, recording and reporting photon beam therapy. ICRU Report No 50. Bethesda, MD: ICRU; 1993.
40. ICRU International Commission on Radiation Units and Measurements. Prescribing, recording and reporting photon beam therapy. ICRU Report No 62. Bethesda, MD: ICRU; 1999.
41. IAEA International Atomic Energy Agency. Absorbed dose determination in photon and electron beams - An international code of

practice. IAEA Technical Report Series No. 277. Vienna: IAEA; 1987 (2nd edition in 1997).
42. Huang PH, Kase KR, Bjärngard BE. Spectral characterization of 4 MV Bremsstrahlung by attenuation analysis. *Med Phys*. 1981; **8**: 368-374.
43. Yu MK, Sloboda S, Murray B. Linear accelerator photon beam quality at off-axis points. *Med Phys*. 1997; **24**: 233-239.
44. Brahme A, Andreo P. Dosimetry and quality specification of high energy photon beams. *Acta Radiol Oncol*. 1986; **25**: 213-223.
45. Zhu Y, Van Dyk J. Accuracy requirements of the primary x-ray spectrum in dose calculations using FFT convolution techniques. *Med Phys*. 1995; **22**: 421-426.
46. ICRU International Commission on Radiation Units and Measurements. Dosimetry of High-Energy Photon Beams based on Standards of Absorbed Dose to Water, ICRU Report 64. Kent: Nuclear Technology Publishing; 2001.
47. Andreo P. Dosimetry of high-energy photon beams. Present status and future prospects for the data used in ionization chamber dosimetry. Report RI 1991-03, Radiation Physics Department, University of Stockholm; 1991.
48. Baker CR. Reconstruction of clinical bremsstrahlung spectra in the range 4 to 30 MeV. PhD Thesis, Faculty of Science at the University of Surrey; 1993.
49. Kosunen A, Rogers DW. Beam quality specification for photon beam dosimetry. *Med Phys*. 1993; **20**: 1181-1188.
50. Nisbet A, Weatherburn H, Fenwick JD, McVey G. Spectral reconstruction of clinical megavoltage photon beams and the implications of spectral determination on the dosimetry of such beams. *Phys Med Biol*. 1998; **43**: 1507-1521.
51. Rogers DW. Correcting for electron contamination at dose maximum in photon beams. *Med Phys*. 1999; **26**: 533-537.
52. Rogers DW, Yang CL. Corrected relationship between $\%dd(10)_x$ and stopping-power ratios. *Med Phys*. 1999; **26**: 538-540.
53. Andreo P. On the beam quality specification of high-energy photons for radiotherapy dosimetry. *Med Phys*. 2000; **27**: 434-440.
54. Karlsson M, Nyström H, Svensson H. Photon beam characteristics on the MM50 racetrack microtron and a new approach for beam quality determination. *Med Phys*. 1993; **20**: 143-149.
55. Nyström H, Karlsson M. Photon beam quality specification by narrow-beam transmission measurements. *Phys Med Biol*. 1994; **39**: 1231-1245.
56. Bjärngard BE, Vadash P. Relations between scatter factor, quality index and attenuation for x-ray beams. *Phys Med Biol*. 1998; **43**: 1325-1330.

57. Georg D, Dutreix A. Methods for beam data acquisition offered by a mini-phantom. *Phys Med Biol*. 1999; **44**: 817-832.
58. Rogers DW. Comment on "On the beam quality specification of high-energy photons for radiotherapy dosimetry" [Med. Phys. 27, 434-440 (2000)]. *Med Phys*. 2000; **27**: 441-444.
59. Mohan R, Chui C, Lidofsky L. Energy and angular distributions of photons from medical linear accelerators. *Med Phys*. 1985; **12**: 592-597.
60. McDonough J, Bloch P, Bjärngard BE. Determination of scatter factor parameters and electron disequilibrium for monoenergetic photon beams. *Med Phys*. 1999; **26**: 200-205.
61. Bjärngard BE. Scatter factors for a 25-MV x-ray beam. *Med Phys*. 1993; **1**: 357-361.
62. Siddon RL, Dewyngaert JK, Bjärngard BE. Scatter integration with right triangular fields. *Med Phys*. 1985; **12**: 229-231.
63. Xiao Y, Bjärngard BE, Reiff J. Equivalent fields and scatter integration for photon fields. *Phys Med Biol*. 1999; **44**: 1053-1065.
64. Dunscombe PB, Nieminen JM. On the field-size dependence of relative output from a linear accelerator. *Med Phys*. 1992; **19**: 1441-1444.
65. Meeks SL. Clinical implications of collimator exchange effect, relative collimator and phantom scatter. *Med Dosim*. 1996; **21**: 27-30.
66. Moyer RF. Systematic patient-dose errors for 4- and 10-MeV microwave linear accelerators associated with rectangular collimator settings. *Radiology*. 1978; **129**: 803-806.
67. Weber L, Nilsson P, Ahnesjö A. Build-up cap materials for measurement of photon head-scatter factors. *Phys Med Biol*. 1997; **42**: 1875-1886.
68. Kijewski PK, Chin LM, Bjärngard BE. Wedge-shaped dose distributions by computer-controlled collimator motion. *Med Phys*. 1978; **5**: 426-429.
69. Shackford H, Bjärngard BE, Vadash P. Dynamic universal wedge. *Med Phys*. 1995; **22**: 1735-1741.
70. Knöös T, McDonough J, Bjärngard B. Dose calculations for a dynamic universal wedge. WiP AAPM. 1997.
71. Bjärngard BE, Vadash P, Zhu T. Doses near the surface in high-energy x-ray beams. *Med Phys*. 1995; **22**: 465-468.
72. Nizin PS. Electronic equilibrium and primary dose in collimated photon beams. *Med Phys*. 1993; **20**: 1721-1729.
73. Biggs PJ, Ling CC. Electrons as the cause of the observed dmax shift with field size in high energy photon beams. *Med Phys*. 1979; **6**: 291-295.

74. Kim S, Liu CR, Zhu TC, Palta JR. Photon beam skin dose analyses for different clinical setups. *Med Phys*. 1998; **25**: 860-866.
75. Nilsson B. Electron contamination from different materials in high energy photon beams. *Phys Med Biol*. 1985; **30**: 139-151.
76. Nilsson B, Brahme A. Absorbed dose from secondary electrons in high energy photon beams. *Phys Med Biol*. 1979; **24**: 901-912.
77. Nilsson B, Brahme A. Electron contamination from photon beam collimators. *Radiother Oncol*. 1986; **5**: 235-244.
78. Petti PL, Goodman MS, Gabriel TA, Mohan R. Investigation of buildup dose from electron contamination of clinical photon beams. *Med Phys*. 1983; **10**: 18-24.
79. Petti PL, Goodman MS, Sisterson JM, Biggs PJ, Gabriel TA, Mohan R. Sources of electron contamination for the Clinac-35 25-MV photon beam. *Med Phys*. 1983; **10**: 856-861.
80. Sjögren R, Karlsson M. Electron contamination in clinical high energy photon beams. *Med Phys*. 1996; **23**: 1873-1881.
81. Zhu TC, Palta JR. Electron contamination in 8 and 18 MV photon beams. *Med Phys*. 1998; **25**: 12-19.
82. Fontenla DP, Napoli JJ, Hunt M, Fass D, McCormick B, Kutcher GJ. Effects of beam modifiers and immobilization devices on the dose in the build-up region. *Int J Radiat Oncol Biol Phys*. 1994; **30**: 211-219.
83. Jursinic PA, Mackie TR. Characteristics of secondary electrons produced by 6, 10 and 24 MV x-ray beams. *Phys Med Biol*. 1996; **41**: 1499-1509.
84. Malataras G, Kappas C, Lovelock DM. A monte carlo approach to electron contamination sources in the Saturne-25 and -41. *Phys Med Biol*. 2001; **46**: 2435-2446.
85. Sheikh-Bagheri D, Rogers DW, Ross CK, Seuntjens JP. Comparison of measured and Monte Carlo calculated dose distributions from the NRC linac. *Med Phys*. 2000; **27**: 2256-2266.
86. Klein EE, Purdy JA. Entrance and exit dose regions for a Clinac-2100C. *Int J Radiat Oncol Biol Phys*. 1993; **27**: 429-435.
87. Mackie TR, Scrimger JW. Contamination of a 15-MV photon beam by electrons and scattered photons. *Radiology*. 1982; **144**: 403-409.
88. Rao BM, Prasad SG, Parthasaradhi K, Lee Y, Ruparel R, Garces R. Investigations on the near surface dose for three 10-MV x-ray beam accelerators with emphasis on the reduction of electron contamination. *Med Phys*. 1988; **15**: 246-249.
89. Beauvais H, Bridier A, Dutreix A. Characteristics of contamination electrons in high energy photon beams. *Radiother Oncol*. 1993; **29**: 308-316.

90. Purdy JA. Buildup/surface dose and exit dose measurements for a 6-MV linear accelerator. *Med Phys*. 1986; **13**: 259-262.
91. Velkley DE, Manson DJ, Purdy JA, Oliver Jr GD. Build-up region of megavoltage photon radiation sources. *Med Phys*. 1975; **2**: 14-19.
92. Shih R, Li XA, Hsu WL. Dosimetric characteristics of dynamic wedged fields: a Monte Carlo study. *Phys Med Biol*. 2001; **46**: N281-N292.
93. Venselaar J, Heukelom S, Jager N, Mijnheer B, van der Laarse R, van Gasteren H, van Kleffens H, Westermann C. Effect of electron contamination on scatter correction factors for photon beam dosimetry. *Med Phys*. 1999; **26**: 2099-2106.
94. Georg D, Garibaldi C, Dutreix A. Measurements of basic parameters in wedged high-energy photon beams using a mini-phantom. *Phys Med Biol*. 1997; **42**: 1821-1831.
95. Georg D, Garibaldi C, Dutreix A. Output ratios in a miniphantom for asymmetric fields shaped by a multileaf collimator. *Phys Med Biol*. 1997; **42**: 2305-2317.
96. Van Gasteren JJ, Heukelom S, Van Kleffens HJ, Van der Laarse R, Venselaar JL, Westermann CF. The determination of phantom and collimator scatter components of the output of megavoltage photon beams: Measurement of the collimator scatter part with a beam-coaxial narrow cylindrical phantom. *Radiother Oncol*. 1991; **20**: 250-257.
97. Jursinic PA, Thomadsen BR. Measurements of head-scatter factors with cylindrical build-up caps and columnar miniphantoms. *Med Phys*. 1999; **26**: 512-517.
98. Karlsson M, Karlsson M, Sjögren R, Svensson H. Semi-conductor detectors in output factor measurements. *Radiother Oncol*. 1997; **42**: 293-296.
99. ICRU International Commission on Radiation Units and Measurements. Radiation Quantities and Units. ICRU Report 33. Washington, D.C.: ICRU; 1980.
100. ICRU International Commission on Radiation Units and Measurements. Fundamental Quantities and Units for Ionizing Radiation. ICRU Report 60. Bethesda, MD: ICRU; 1998.
101. Johnsson SA, Ceberg CP. Off-axis primary-dose measurements using a mini-phantom. *Med Phys*. 1997; **24**: 763-767.
102. Iwasaki A. Theoretical considerations of using in-air chamber readings for evaluation of the attenuation of in-phantom primary water collision kerma. *J Jpn Soc Ther Radiol Oncol*. 1998; **10**: 47-52.
103. Nelson WR, Hirayama H, Rogers DWO. The EGS4 code system. Report SLAC-265, Stanford Linear Accelerator Center, Stanford, CA. 1985.

104. Basran PS, Ansbacher W, Field GC, Murray BR. Evaluation of optimized compensators on a 3D planning system. *Med Phys*. 1998; **25**: 1837-1844.
105. Hansson H, Björk P, Knöös T, Nilsson P. Verification of a pencil beam based treatment planning system: Output factors for open photon beams shaped with MLC or blocks. *Phys Med Biol*. 1999; **44**: N201-N207.
106. Hurkmans C, Knöös T, Nilsson P. Dosimetric verification of open asymmetric photon fields calculated with a treatment planning system based on dose-to-energy-fluence concepts. *Phys Med Biol*. 1996; **41**: 1277-1290.
107. Hurkmans C, Knöös T, Nilsson P, Svahn Tapper G, Danielsson H. Limitations of a pencil beam approach to photon dose calculations in the head and neck region. *Radiother Oncol*. 1995; **37**: 74-80.
108. Jung B, Montelius A, Dahlin H, Ekström P, Ahnesjö A, Hogstrom B, Glimelius B. The conceptual design of a radiation oncology planning system. *Comput Methods Programs Biomed*. 1997; **52**: 79-92.
109. Knöös T, Ahnesjö A, Nilsson P, Weber L. Limitations of a pencil beam approach to photon dose calculations in lung tissue. *Phys Med Biol*. 1995; **40**: 1411-1420.
110. Knöös T, Ceberg C, Weber L, Nilsson P. The dosimetric verification of a pencil beam based treatment planning system. *Phys Med Biol*. 1994; **39**: 1609-1628.
111. Weber L, Ahnesjö A, Nilsson P, Saxner M, Knöös T. Verification and implementation of dynamic wedge calculations in a treatment planning system based on a dose-to-energy-fluence formalism. *Med Phys*. 1996; **23**: 307-316.
112. Shih R, Li XA, Chu JC. Dynamic wedge versus physical wedge: a Monte Carlo study. *Med Phys*. 2001; **28**: 612-619.
113. Tailor RC, Tello VM, Schroy CB, Vossler M, Hanson WF. A generic off-axis energy correction for linac photon beam dosimetry. *Med Phys*. 1998; **25**: 662-667.

POPULÄRVETENSKAPLIG SAMMANFATTNING

Strålbehandling av cancerpatienter sker idag med avancerad teknik och utrustning. Förberedelserna inför behandlingen är omfattande och kräver medverkan av flera olika personalkategorier och övervakning via datoriserade verifikationssystem. I varje led i förberedelsekedjan finns en potentiell risk för avvikelser, vilka kan vara både systematiska eller tillfälliga i sin natur. Den senare typen av avvikelser orsakas ofta av rena misstag på grund av den ”mänskliga faktorn”. För att undvika felaktigheter där patienten kan komma till skada, är det av största vikt att alla inställningar kontrolleras vid första behandlingstillfället. Framför allt är det viktigt att verifiera att den givna stråldosen överensstämmer med den planerade.

Inom ramen för detta arbete har ett kvalitetssäkringsprogram bestående av ett komplett system för oberoende stråldosberäkningar utvecklats. Den beräkningsmodell som används är helt fristående från det kommersiella system som normalt används för att beräkna stråldosen. Modellen bygger på ett fåtal mätbara parametrar som är direkt kopplade till strålkvaliteten på den aktuella behandingsmaskinen. Just parametrarnas koppling till strålkvalitet och hur dessa parametrar erhålls från mätningar har varit utgångsgpunkten för flera av delarbetena. Trots sin enkelhet klarar modellen av att beräkna stråldoser i mycket avancerade patientgeometrier med en hög noggranhet. Beräkningsmodellens enkelhet gör vidare att den är möjlig att implementera i små handdatorer, vilka kan medföras ute i strålbehandlingskliniken. Dessa handdatorer kan i sin tur kommunicera med behandlingsmaskinernas egna kontrollsystem, vilket gör att man alltid har tillgång till den senaste patientinformationen. Systemet har använts kliniskt under en längre tid och i den efterföljande utvärderingen kunde ett systematiskt fel i patientgeometrin för vissa patientgrupper identifieras. Inga tillfälliga fel upptäcktes. Vidare framgick det att den aktionsnivå som tidigare satts var för hög vid vissa typer av behandlingar. Utvärderingen visade också att handdatorn är ett utmärkt verktyg med vilken man kan utföra oberoende, avancerade och effektiva kontroller av stråldosen till patienen vid första behandlingstillfället. Systemet används numera rutinmässigt på strålbehandlingskliniken vid Lunds Universitetssjukhus och på Radioterapikliniken vid Rigshospitalet i Köpenhamn och kommer inom kort också att implementeras på andra kliniker i Sverige.